Col. Stapp.

CONFIDENTIAL

Copy 262
RM L57J16

NACA RM L57J16

12 FEB 1958
16401

TECH LIBRARY KAFB, NM
0144739

7810

NACA

RESEARCH MEMORANDUM

EFFECT OF TARGET-TYPE THRUST REVERSER ON TRANSONIC AERODYNAMIC CHARACTERISTICS OF A SINGLE-ENGINE FIGHTER MODEL

By John M. Swihart

Langley Aeronautical Laboratory
Langley Field, Va.

CLASSIFIED DOCUMENT

This material contains information affecting the National Defense of the United States within the meaning of the espionage laws, Title 18, U.S.C., Secs. 793 and 794, the transmission or revelation of which in any manner to an unauthorized person is prohibited by law.

NATIONAL ADVISORY COMMITTEE FOR AERONAUTICS

WASHINGTON
January 13, 1958

CONFIDENTIAL

Class[illegible] cancelled (or changed to Unclassified)

By authority of NASA Tech Pub Announcement #17
(OFFICER AUTHORIZED TO CHANGE)

By ..... 14 Apr. 60
NAME AND

..... NK
GRADE OF OFFICER MAKING CHANGE)

16 Feb. 61
DATE

TECH LIBRARY KAFB, NM
0144739

NATIONAL ADVISORY COMMITTEE FOR AERONAUTICS

RESEARCH MEMORANDUM

EFFECT OF TARGET-TYPE THRUST REVERSER ON TRANSONIC AERODYNAMIC CHARACTERISTICS OF A SINGLE-ENGINE FIGHTER MODEL

By John M. Swihart

SUMMARY

A brief investigation of a target-type thrust reverser on a single-engine fighter model has been conducted in the Langley 16-foot transonic tunnel at Mach numbers from 0.20 to 1.05. At Mach numbers of 0.80, 0.92, and 1.05, a hydrogen peroxide turbojet-engine simulator was operated with the thrust reverser extended. The angle of attack was varied from 0° to 5° at these Mach numbers. The Reynolds number of the free stream, based on the mean aerodynamic chord, was about 5×10^{6}.

It was estimated that reversed jet operation separated the model boundary-layer flow over the upper surface of the horizontal tail and upper part of the afterbody. This resulted in a positive pitch increment due to reversed jet operation. Jet-on operation also tended to stabilize the severe lateral oscillations which occurred with the reverser extended and the jet off. It appeared that these jet-off oscillations were the result of an alternating separation and reattachment of the flow on the rearmost portions of the fuselage afterbody.

INTRODUCTION

There has been considerable interest recently in the use of thrust reversers to shorten the landing roll of turbojet-powered aircraft. Several investigations of many different types and shapes of thrust reversers have been made in still air. (For example, see refs. 1 to 5.) Taxi tests of a cascade-type reverser installed on a single-engine fighter airplane have been reported in reference 6. In addition to the interest in the thrust reverser as a landing aid, there has been an interest expressed in using the thrust reverser as a speed brake. It might be used for combat maneuvering, steep descent from high altitude, and during the approach to landing (ref. 7). Some of these flight regimes were investigated several years ago at speeds up to 280 miles per hour with

a fighter-type airplane which had both a piston engine and a small turbojet engine. The results of those flight tests are reported in references 8 and 9.

It is the purpose of this paper to present the results of a brief wind-tunnel investigation to study the aerodynamic phenomena associated with a target-type thrust reverser on a single-engine fighter model. This investigation was conducted in the Langley 16-foot transonic tunnel at Mach numbers from 0.20 to 1.05 at 0° angle of attack. Power-on effects with the reverser extended were obtained through the angle-of-attack range from 0° to 5° at Mach numbers of 0.80, 0.92, and 1.05. The turbojet exhaust was simulated with a hydrogen peroxide gas-generator system and this technique is described in reference 10.

SYMBOLS

All forces and moments presented are for the fuselage-tail combination and do not include the wing.

A	area
AR	aspect ratio
b	wing span
C_D	drag coefficient, $D/q_{\infty}S$
C_L	lift coefficient, $L/q_{\infty}S$
C_l	rolling-moment coefficient, $L'/q_{\infty}Sb$
C_m	pitching-moment coefficient, $M/q_{\infty}Sc'$
C_n	yawing-moment coefficient, $N/q_{\infty}Sb$
C_Y	lateral-force coefficient, $Y/q_{\infty}S$
C_p	pressure coefficient, $\frac{p_{local} - p_{\infty}}{q_{\infty}}$
c	local chord
c'	wing mean aerodynamic chord

D	drag of fuselage-tail combination
d	diameter
H_2O_2	hydrogen peroxide (90 percent concentration by weight)
L	lift of fuselage-tail combination
L'	rolling moment of fuselage-tail combination
l	afterbody length, measured from base, positive rearward
M	Mach number or pitching moment of fuselage-tail combination referred to 0.25c'
m	mass flow
N	yawing moment of fuselage-tail combination referred to 0.25c'
p	pressure, abs
q	dynamic pressure
S	wing area, includes area covered by fuselage
V	velocity
Y	lateral force of fuselage-tail combination
α	angle of attack of fuselage-tail combination
ϕ	meridian angle measured clockwise from top center line looking upstream, deg

Subscripts:

b	base
t	total
i	internal
j	jet
e	exit
∞	free-stream conditions

bal	balance measured
p	primary
s	secondary
r	reverser
1,2,3	axial stations (fig. 3(c))

APPARATUS AND METHODS

Tunnel

The Langley 16-foot transonic tunnel is a single-return atmospheric wind tunnel with an octagonal slotted-throat test section. The operational and power characteristics are described in reference 11. The bifurcate sting support system used for this model is described in reference 12.

Model

The single-engine turbojet fighter model used for this investigation was the same model described in reference 12. Figure 1 shows the model with and without the thrust reverser. Figure 2 shows a dimensional sketch of the target-type thrust reverser. The reverser was designed for about 60-percent reverse thrust by using the design charts for target-type reversers shown in reference 3. The reverser was located 1.18 inches downstream of the model base.

Figure 3 is a cutaway view of the model and the support system. The geometric characteristics of the wings, tails, and fuselage are given in the figure. The model was constructed of stainless steel and aluminum, and the wing forms an integral part of the support system. Figure 3 shows that the wing was rigidly attached to the bifurcate sting support and the fuselage-tail assembly was mounted on a six-component strain-gage balance supported by the wing. Flexible diaphragm seals were used at the juncture between the wing and the fuselage. The H_2O_2 turbojet simulator was also supported from the wing in such a manner that the thrust and drag were measured separately. The details of these two systems will be discussed later.

Tests

The model was investigated at Mach numbers from 0.20 to 1.05 at 0° angle of attack. In addition, the angle-of-attack range was from 0° to 5° at Mach numbers of 0.80, 0.92, and 1.05. The Reynolds number based on c' was about 5×10^{6} for this Mach number range. The model was investigated with the reverser off, simulating retraction into the sides of the fuselage, and with the reverser fully extended. The H_2O_2 turbojet simulator was operated over a jet-total-pressure-ratio range from 1.0 (jet off) to 5 at Mach numbers of 0.80 and above. The technique for obtaining jet-on data is described in reference 12. Tuft studies were made over the boattail with and without jet flow and with and without the reverser. In addition, for one test, the reverser was perforated with 18 holes (fig. 1(f)).

Instrumentation

Pressures were measured at several nominal meridian angles around the fuselage and for about 3 primary jet diameters ahead of the base. Table I shows the location of each of these pressure orifices. Pressure tubing from each orifice was conducted out of the fuselage through the wing and bifurcate sting support and connected to electrical pressure transducers located in the sting barrel. Eighty electrical pressure transducers of the type described in reference 13 were manifolded to a common reference pressure and this whole transducer manifold system was immersed in a constant-temperature bath. This constant-temperature bath kept the zero and sensitivity shifts of the electrical pressure transducers to a minimum.

In addition to the external pressures, primary jet total and static pressures, secondary inlet and exit total and static pressures, and primary jet and secondary air total temperatures were measured.

Fuselage-tail forces and moments were obtained on a six-component strain-gage balance and thrust forces were obtained on a one-component thrust balance.

The angle of attack of the fuselage was measured by a calibrated pendulum strain-gage attitude indicator mounted in the canopy. The resulting angles of attack are independent of sting and balance deflections due to load.

Data Reduction

The electrical signals from the pressure transducers were transmitted to carrier amplifiers and then to recording oscillographs located

in the tunnel control room. The trace deflections on the recorder film were converted to pressures, forces, moments, and temperatures by machine computation. The pressures, forces, and moments were also converted by machine computation to standard coefficients.

It is of interest to note that four recording oscillographs were used and that all four recorders were synchronized by a timing device. In this manner the H_2O_2 simulator operator started all recorders together, marked each data point on the films of each simultaneously, and stopped all recorders together; therefore, all data presented herein for a given point were obtained simultaneously.

Drag system.- The external drag of the fuselage-tail assembly is defined as the sum of all pressure and viscous forces acting on the external surface of the model and across the base to the edge of the ejector. (See fig. 3(c).) The measured-external-drag equation is as follows:

$$D = D_{bal} + \left(p_i - p_\infty\right)\left[A_2 - \frac{1}{2}\left(A_2 + A_1\right)\right] - \left(p_b - p_\infty\right)\left[\frac{1}{2}\left(A_2 + A_1\right) - A_e\right]$$

Figure 3(b) shows the location of the six-component strain-gage balance and figure 3(c) shows areas and pressure locations.

Inspection of the drag equation indicates a pressure force across the flexible diaphragm seal (figs. 3(b) and 3(c)). This force was only a small fraction of the measured drag and the exact disposition between the drag and thrust systems was unknown; however, one-half of the small pressure force across the flexible seal was arbitrarily charged to each system. The external drag is also charged with the small internal drag of the secondary air duct from the nose to the flexible bellows where the duct is connected to the thrust system.

Thrust system.- The thrust system is shown by the sketch in figure 3(c). The target-type thrust reverser was connected directly to the ejector shroud for this investigation and the thrust measured with the reverser extended should have included the drag of the reverser as well as the reverse thrust.

Unfortunately, the thrust-balance readings obtained during the investigation were completely unreliable and could not be used to obtain a measure of the reverse thrust or drag of the reverser.

Accuracy

The estimated accuracies of the data presented in this paper are given as follows:

C_D	±0.001
C_L	±0.005
C_l	±0.001
C_m	±0.001
C_n	±0.001
C_Y	±0.002
C_p	±0.01
M	±0.005
α	±0.1
$p_{t,j}/p_\infty$	±0.2

RESULTS AND DISCUSSION

Pressure Data, Lateral Oscillations, and Tuft Pictures

Probably the most interesting aerodynamic phenomenon observed in this brief investigation was a rather violent lateral oscillation of the model with the jet off. These lateral oscillations were observed from about $M = 0.20$ to $M = 1.05$. In order to observe the flow disturbances which might be causing these oscillations, tufts were applied to the upper half of the fuselage and part of the horizontal tails. (See figs. 1(e) and 1(f).) A motion-picture camera was installed to photograph these tufts and an observer also watched the model. By coordination between the observer and the model control operators, it was possible at a Mach number of 0.92 to obtain simultaneous force data, pressure data, and motion pictures of the tufts.

Figure 4 shows the oscillograph record of the forces and moments obtained at this point with the reverser extended and the jet off. This record is typical of all data obtained with the jet off when the reverser was extended. The tuft pictures taken by the motion-picture camera at the two selected data points are also shown in figure 4. At the first point, the lateral force was positive (lateral trace towards top of record is positive), the yawing moment was negative (yaw trace toward top of record is negative, note $M = 0$ trace positions), and the tufts were lying at an appreciable angle to the free-stream direction on the left side of the afterbody and in the free-stream direction on the right side of the afterbody. At the second point, the lateral force is negative, the yawing moment is positive, and the tufts have reversed positions.

Figure 4(b) shows the variation of pressure coefficient with afterbody length in jet diameters for several meridians at the two data points. The pressures at the first point are generally more positive and more asymmetric than those shown for the second point, especially between $l/d_j = 0$ and $l/d_j = -2.0$. Since the tufts on the left side were skewed at the first point and the pressures are more positive, it is believed that an alternating separation and a reattachment were occurring on the rear parts of the afterbody for about 2 jet diameters ahead of the base $\left(l/d_j < -2.0\right)$. Attempts were made to stabilize this separation by attaching a 1/8-inch-diameter wire to the fuselage just ahead of the horizontal tail and by perforating the reverser as shown in figure 1(f). Neither of these changes had any effect on the separation and the resulting lateral oscillations.

It may be of some interest to note that although the time shown on the record (fig. 4(a)) for the side force and yawing moment to change sign is of the order of 1 second, the motion-picture camera was operating at 24 frames per second, and the tufts were completely changed between two consecutive frames. This means that the last ring of tufts shown in figure 4(a) (left picture) changed from a steady alinement with the stream to an angle of about 45° to the stream (right picture) in 1/24 second and the tufts were fairly steady at that angle.

It is believed that this irregular alternating separation and reattachment will occur with any reverser of this type when the jet is off, since this alternating irregular vortex pattern is a phenomenon of a turbulent boundary layer (ref. 14) and is often observed in separated flows. The rapid changes in lateral force and yawing moment due to this flow pattern might make an airplane uncontrollable, since these changes are the equivalent of about 5° of change in yaw angle. If the period of the oscillation could be controlled by the pilot, the magnitude of the deflection and accompanying shaking of the airframe would at least be very disconcerting and undesirable.

Figure 5 shows a sketch made with the aid of photographs of the tufts at a Mach number of 0.80 with the jet on and off. In figure 5(b) the tufts are completely reversed for about 3 jet diameters ahead of the base and some outflow is indicated on the horizontal tail. It is believed that the reversed jet flow was attached to the fuselage at least in the vicinity of the base and forward about 1 jet diameter since the fuselage was discolored from heat in this region. The jet probably extended forward for 3 jet diameters before turning outward and backward to the free-stream direction. This path of the jet will be discussed later in the presentation of the force data.

Figure 6 shows the variation of C_p with l/d_j for three Mach numbers and three pressure ratios at $\alpha = 0°$. The average afterbody

pressure coefficients for the reverser off are shown for comparison with the measured pressure coefficients for the reverser fully extended. Average C_p is the average of the pressure coefficients at each value of l/d_j. When the jet is off, the data are quite similar at $M = 0.80$ but the pressure coefficients become generally more positive with the reverser extended when the Mach number is increased to 0.92 and 1.05. With the jet operating, the pressures are more positive over the whole of the instrumented afterbody, with the largest difference shown for $M = 1.05$ and $p_{t,j}/p_\infty = 5.0$. At angles of attack of 3.5° and 5°, the pressures became more asymmetric. Figure 7 shows the pressure data at $\alpha = 5^\circ$, $M = 0.92$, and at pressure ratios of 1 and 5.0, and also shows a comparison of the data with the reverser off. These data are typical for all Mach numbers and pressure ratios.

Force and Moment Data

Figure 8 shows the force and moment coefficients plotted against angle of attack for constant values of pressure ratio at $M = 0.80$, 0.92, and 1.05. The data for the model with the reverser off are included for comparison. The effect of the reversed jet on the fuselage-tail drag coefficients was to reduce the values to zero or even slight thrust values at the subsonic Mach numbers. The reduction in drag coefficient due to jet operation was about constant at all Mach numbers and showed the expected increase in C_D with angle of attack. These reductions are probably the result of the fairly large positive pressures being induced on the base and afterbody. (See figs. 6 and 7.)

Figure 6 indicates that the pressures along the bottom of the fuselage (rows 4 and 5) are generally not affected by the jet as much as those at the top (rows 2 and 3). The reverser is mounted relatively high on the fuselage (see fig. 1(d)) and it would be expected that most of the reversed jet effect would be seen above the horizontal tail. It is estimated that the reversed jet has separated the model boundary-layer flow from the upper part of the afterbody (evidenced by high positive pressure-coefficient values) and on the upper surface of the horizontal tail. These observations are consistent with the reversed jet boundary shown in figure 5(b). This positive pressure field above the tail would cause the tail to develop negative lift and produce a positive pitch increment. These are the trends indicated by the force and moment data (fig. 8(a)) at all angles of attack.

Figure 8(b) shows the rolling-moment, lateral-force, and yawing-moment coefficients. There is only a very small effect on rolling moment for all conditions. This indicates that the reversed-flow field was probably fairly symmetrical about the model vertical center line. The oscillatory nature of the lateral-force and yawing-moment coefficients

has been discussed previously for the jet-off condition. In general, operating the jet seemed to stabilize the flow to some extent, but when the pressure ratio was increased to 5.0 there was a tendency to return toward the jet-off values. No plausible explanation for this behavior can be found, but it might be caused by a very slight misalinement of the reverser from a plane perpendicular to the free stream.

No shadowgraph pictures were obtained with this model but the observer made sketches of the shock patterns around the afterbody and tail at a Mach number of 1.05. When the jet was off, the horizontal-tail trailing-edge shock was located just ahead of the model base (note positive C_p shift at $l/d_j = -1.2$, fig. 6(c)); however, when the jet was on, the shock was forced forward to a position just ahead of the horizontal tail. No attempt has been made at analyzing the effect of these shock positions on the data and these observations are only included for the reader's information.

Aerodynamic characteristics at lower Mach numbers.- Figure 9 shows the aerodynamic forces and moments on the fuselage-tail combination at $\alpha = 0^{\circ}$ with the jet off at Mach numbers from about 0.40 to 0.80. No reversed-jet flow data were obtained in this Mach number range (below $M = 0.80$) and these data are presented mainly to show the trends at these lower Mach numbers.

Reverse-thrust characteristics.- Unfortunately, as was stated earlier, no reliable reverse-thrust data were obtained during the investigation. In order to detail some of the forces acting on the reverser, a small-scale model of the reverser was constructed, instrumented with pressure tubing, and investigated over the Mach number range from 0.80 to 1.05. (See fig. 10.) These data indicate that the pressure drag on the downstream side of the reverser is approximately doubled when the jet is operating. This indicates that a sizable drag force will also be applied to the airplane in addition to the amount of reversed thrust.

Inspection of figures 1(c) and 1(e) will show two different sizes of supporting members for the reverser. It might be of value to a designer to know that the smaller supports were designed for 100-percent reverse thrust and had a safety factor of 3. These supports failed under the severe oscillating loads imposed on the reverser before the tunnel could be brought up to a Mach number of 0.80. Specifically they failed before any reverse thrust was imposed on them. The larger supports were made more than four times as strong as the smaller ones and no failures occurred with these struts. This information is presented to show the severity of the flow oscillations on this model with the reverser extended.

CONCLUDING REMARKS

A brief investigation of a target-type thrust reverser on a single-engine fighter model has been conducted in the Langley 16-foot transonic tunnel at Mach numbers from 0.20 to 1.05 at 0° angle of attack. Jet-on data were obtained at Mach numbers of 0.80, 0.92, and 1.05 and the angle of attack was varied from 0° to 5° at these Mach numbers.

It is estimated that reversed jet operation separated the model boundary-layer flow over the upper surface of the horizontal tail and on a large extent of the upper part of the afterbody. This resulted in a positive pitch increment due to reversed jet operation. When the reverser was extended with the jet off, severe model lateral oscillations occurred. It appeared that this behavior was the result of an alternating separation and reattachment of the flow on the rearmost portions of the afterbody. The lateral-force and yawing-moment oscillations associated with this flow phenomenon might make an airplane uncontrollable. Reversed jet operation stabilized these flow oscillations somewhat and the lateral coefficients were reduced. An investigation of a small-scale reverser indicated that the pressure drag on the downstream side of the reverser approximately doubled when the jet was operated.

Langley Aeronautical Laboratory,
National Advisory Committee for Aeronautics,
Langley Field, Va., September 27, 1957.

REFERENCES

1. Henzel, James G., Jr., and McArdle, Jack G.: Preliminary Performance Data of Several Tail-Pipe-Cascade-Type Model Thrust Reversers. NACA RM E55F09, 1955.

2. Steffen, Fred W., and McArdle, Jack G.: Performance Characteristics of Cylindrical Target-Type Thrust Reversers. NACA RM E55I29, 1956.

3. Povolny, John H., Steffen, Fred W., and McArdle, Jack G.: Summary of Scale-Model Thrust-Reverser Investigation. NACA TN 3664, 1956.

4. Watson, K. E., and Leitner, M. I.: Reverse Thrust for Turbojet-Engine-Propelled Aircraft. WADC Tech. Rep. 55-301 (Contract No. AF 33(616)-2412), Wright Air Dev. Center, U. S. Air Force, Sept. 1955. (Available from ASTIA as AD No. 91708.)

5. Muller, Charles H.: Performance and Pressure Loadings for the "Vaned Fishmouth" and the "J65-W-7 Prototype" Scale Model Thrust Reversers. Rep. No. 21, Curtiss-Wright Corp., Res. Div. (Clifton, N. J.), Dec. 5, 1956.

6. Kohl, Robert C., and Algranti, Joseph S.: Investigation of a Full-Scale, Cascade-Type Thrust Reverser. NACA TN 3975, 1957.

7. Datner, Paul P.: Thrust-Reverser Devices. Aero. Eng. Rev., vol. 16, no. 7, July 1957, pp. 44-49.

8. Polak, I. P.: Development of Turbo-Jet Engine Thrust Destroying and Reversing Nozzle No. AEL 102. Rep. No. AEL-1108 (Project TED Nos. NAM-PP-375 and NAM-04614), Naval Air Material Center, NAES (Philadelphia), Jan. 13, 1950.

9. Polak, I.: Test of Engineering and Research Corporation Thrust Reverser Part No. 6130 SK-26. Rep. No. AEL-1137 (Project TED No. NAM-PP-375), Naval Air Material Center, NAES (Philadelphia), Aug. 4, 1950.

10. Runckel, Jack F., and Swihart, John M.: A Hydrogen Peroxide Turbojet-Engine Simulator for Wind-Tunnel Powered-Model Investigations. NACA RM L57H15, 1957.

11. Ward, Vernon G., Whitcomb, Charles F., and Pearson, Merwin D.: Air-Flow and Power Characteristics of the Langley 16-Foot Transonic Tunnel With Slotted Test Section. NACA RM L52E01, 1952.

12. Norton, Harry T., Jr., and Swihart, John M.: Effect of a Hot-Jet Exhaust on Pressure Distributions and External Drag of Several Afterbodies on a Single-Engine Airplane Model at Transonic Speeds. NACA RM L57J04, 1957.

13. Patterson, John L.: A Miniature Electrical Pressure Gage Utilizing a Stretched Flat Diaphragm. NACA TN 2659, 1952.

14. Hoerner, Sighard F.: Aerodynamic Drag. Publ. by the author (148 Busteed, Midland Park, N. J.), 1951.

TABLE I.- PRESSURE-ORIFICE LOCATIONS ON AFTERBODY

$[d_j = 2.615 \text{ in.}]$

Row 1			Row 2			Row 3			Row 4			Row 5		
ϕ, deg	l, in.	l/d_j	ϕ, deg	l, in.	l/d_j	ϕ, deg	l, in.	l/d_j	ϕ, deg	l, in.	l/d_j	ϕ, deg	l, in.	l/d_j
326	-8.242	-3.15	290	-8.242	-3.15	260	-8.242	-3.15	226	-8.242	-3.15	180	-8.242	-3.15
326	-6.375	-2.44	294	-6.375	-2.44	261	-6.375	-2.44	228	-6.375	-2.44	180	-6.375	-2.44
326	-4.475	-1.71	280	-4.475	-1.71	262	-4.475	-1.71	222	-4.475	-1.71	180	-5.042	-1.93
326	-2.808	-1.07	280	-2.808	-1.07	262	-2.808	-1.07	222	-2.808	-1.07	180	-3.175	-1.21
326	-1.708	-0.65	280	-1.708	-0.65	262	-1.708	-0.65	222	-1.708	-0.65	180	-2.235	-0.85
326	-0.400	-0.15	280	-0.400	-0.15	262	-0.400	-0.15	222	-0.400	-0.15	185	-1.708	-0.65
352	0	0	306	0	0	262	0	0	232	0	0	199	-0.400	-0.15
												186	0	0

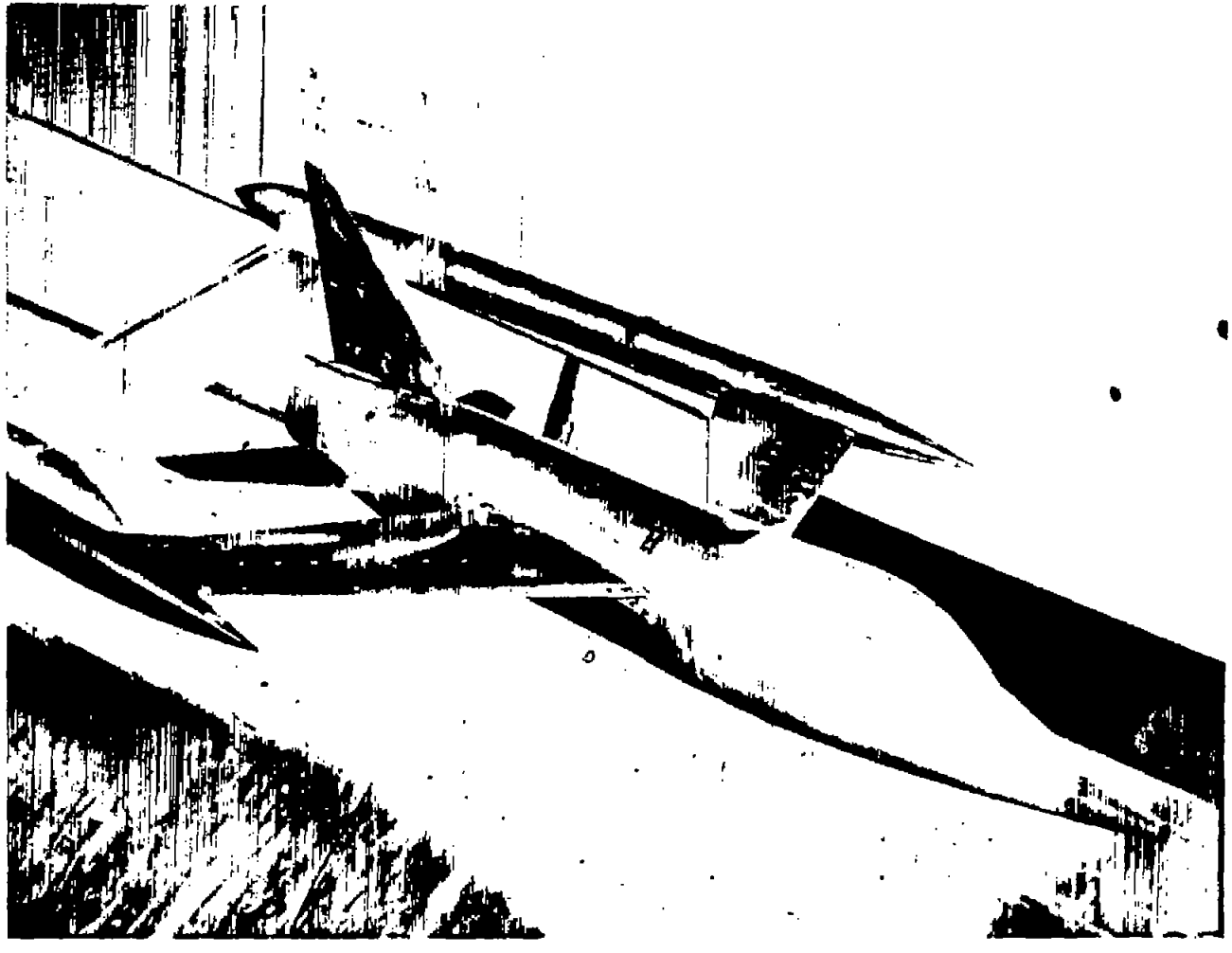

(a) Three-quarter front view, reverser off. L-92106

Figure 1.- Model mounted in test section of Langley 16-foot transonic tunnel.

CONFIDENTIAL

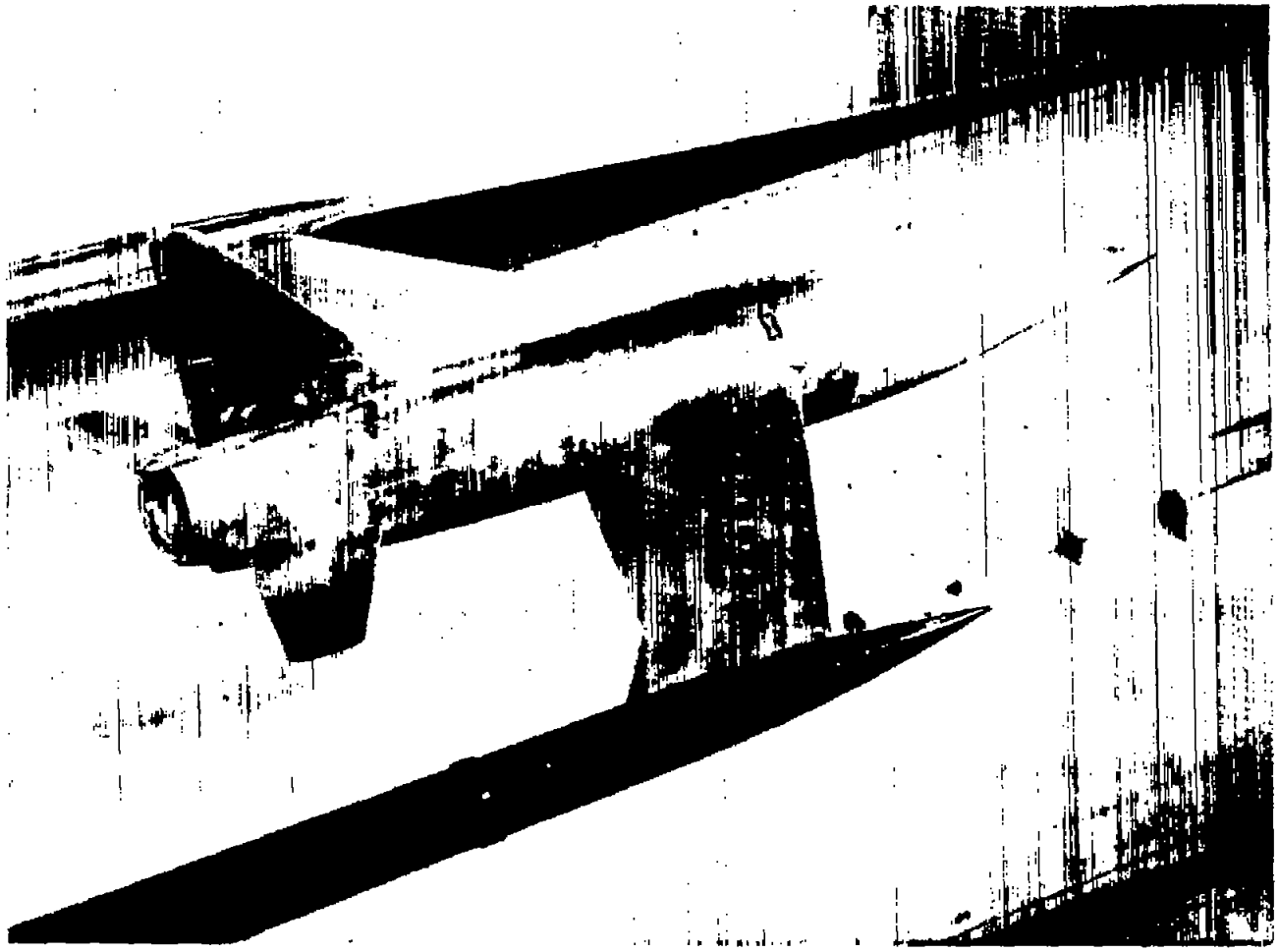

(b) Three-quarter rear view, reverser off. L-92107

Figure 1.- Continued.

CONFIDENTIAL

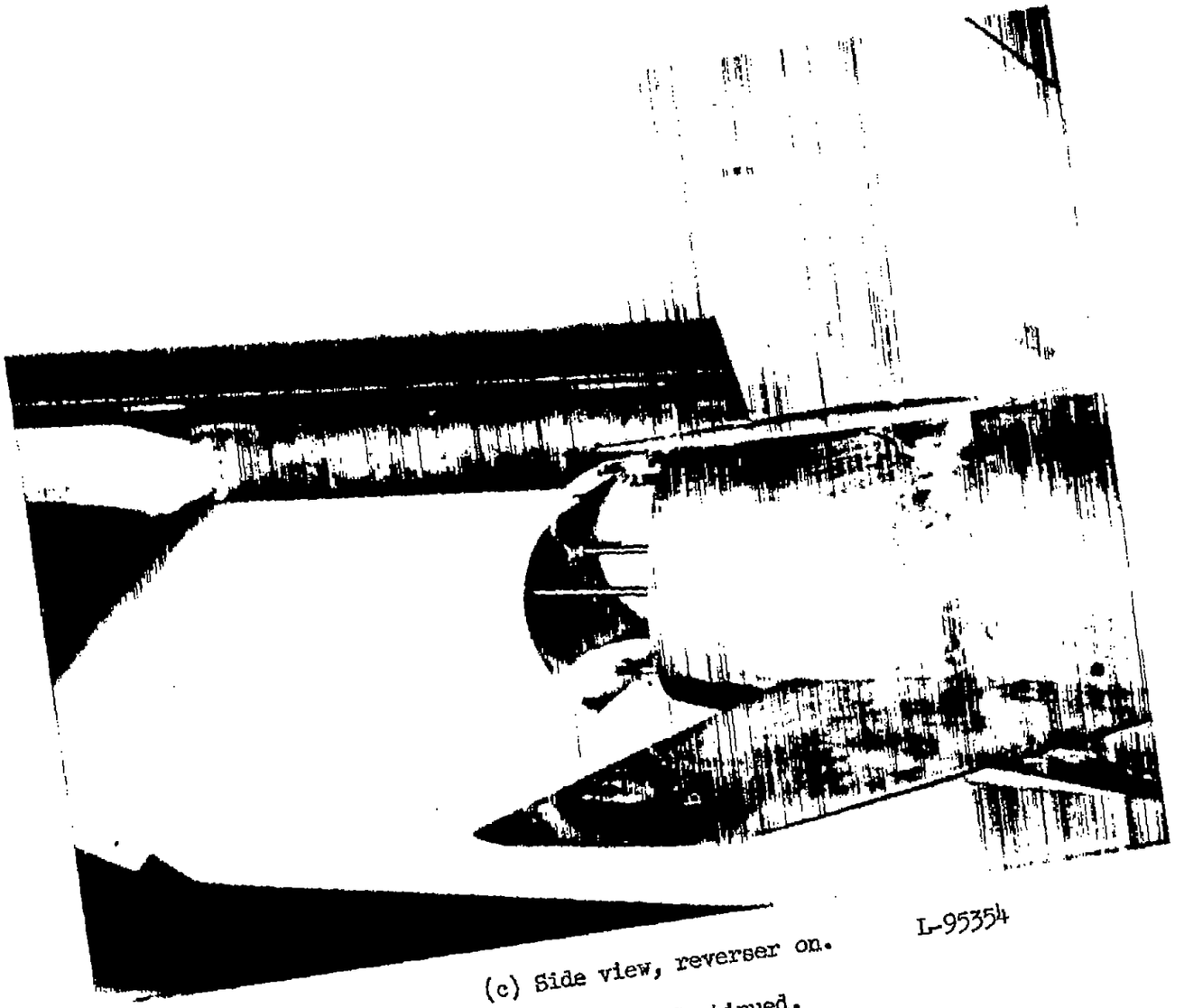

L-95354

(c) Side view, reverser on.

Figure 1.- Continued.

CONFIDENTIAL

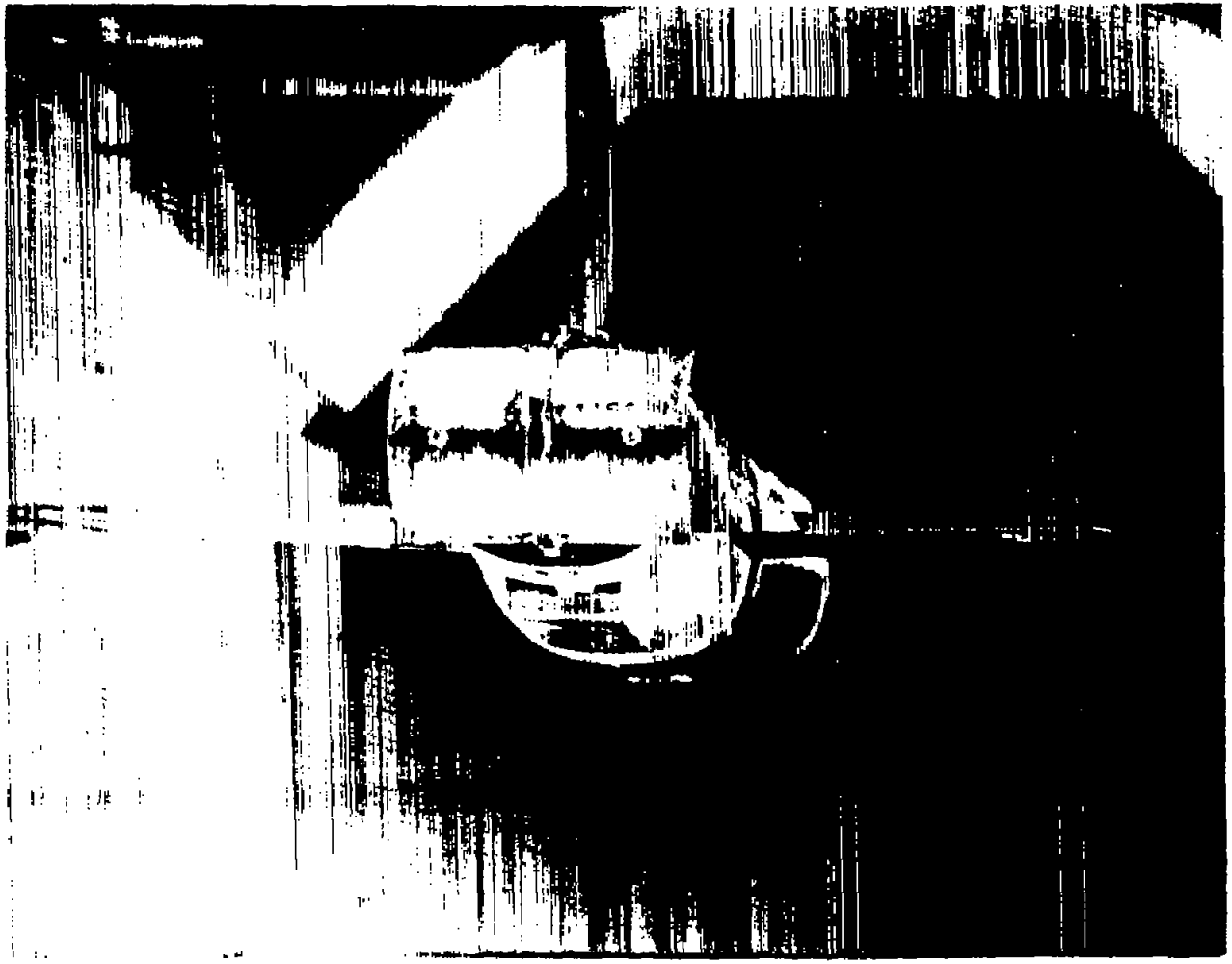

(d) Rear view, reverser on. L-95356

Figure 1.- Continued.

CONFIDENTIAL

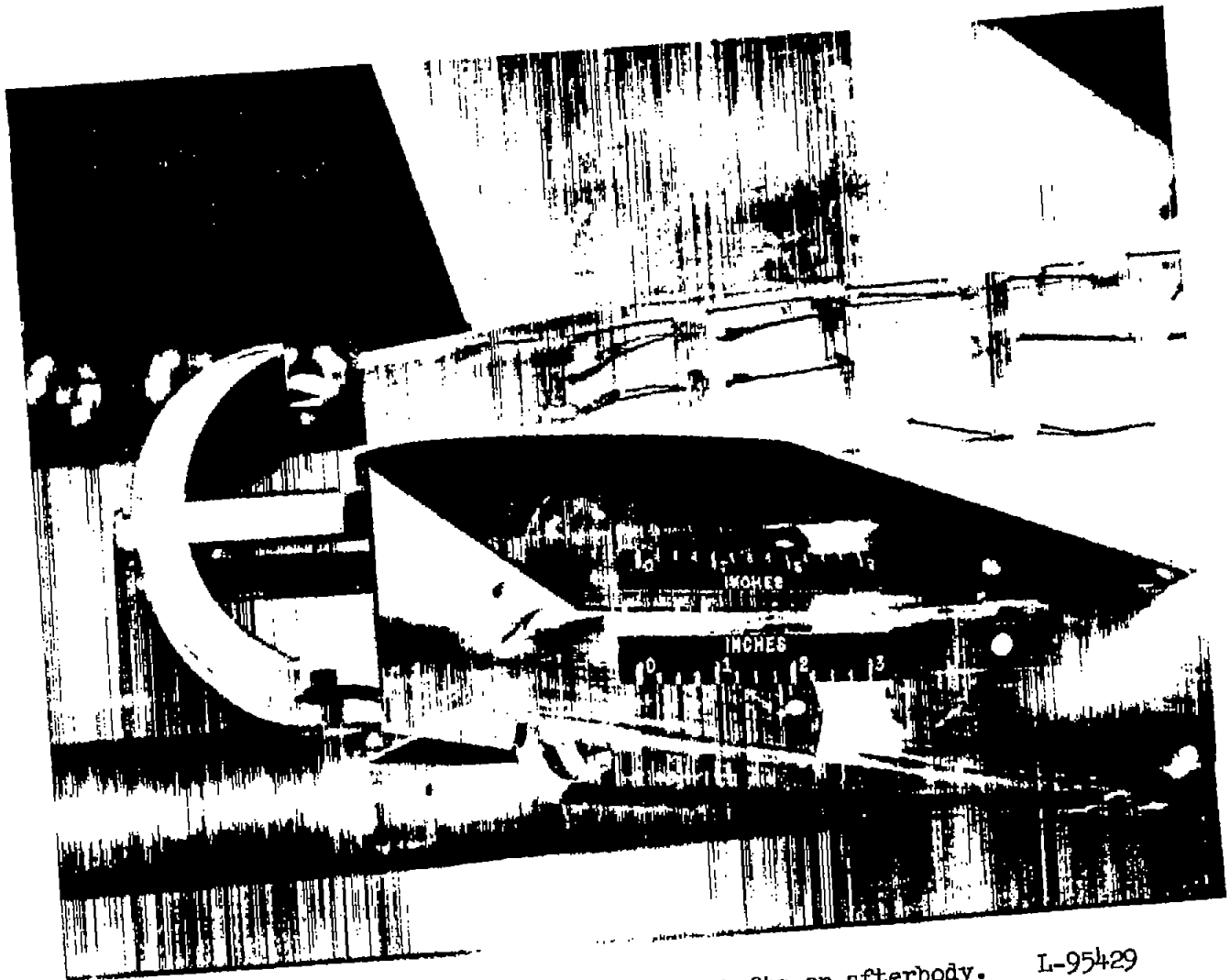

L-95429

(e) Side view, reverser on and tufts on afterbody.

Figure 1.- Continued.

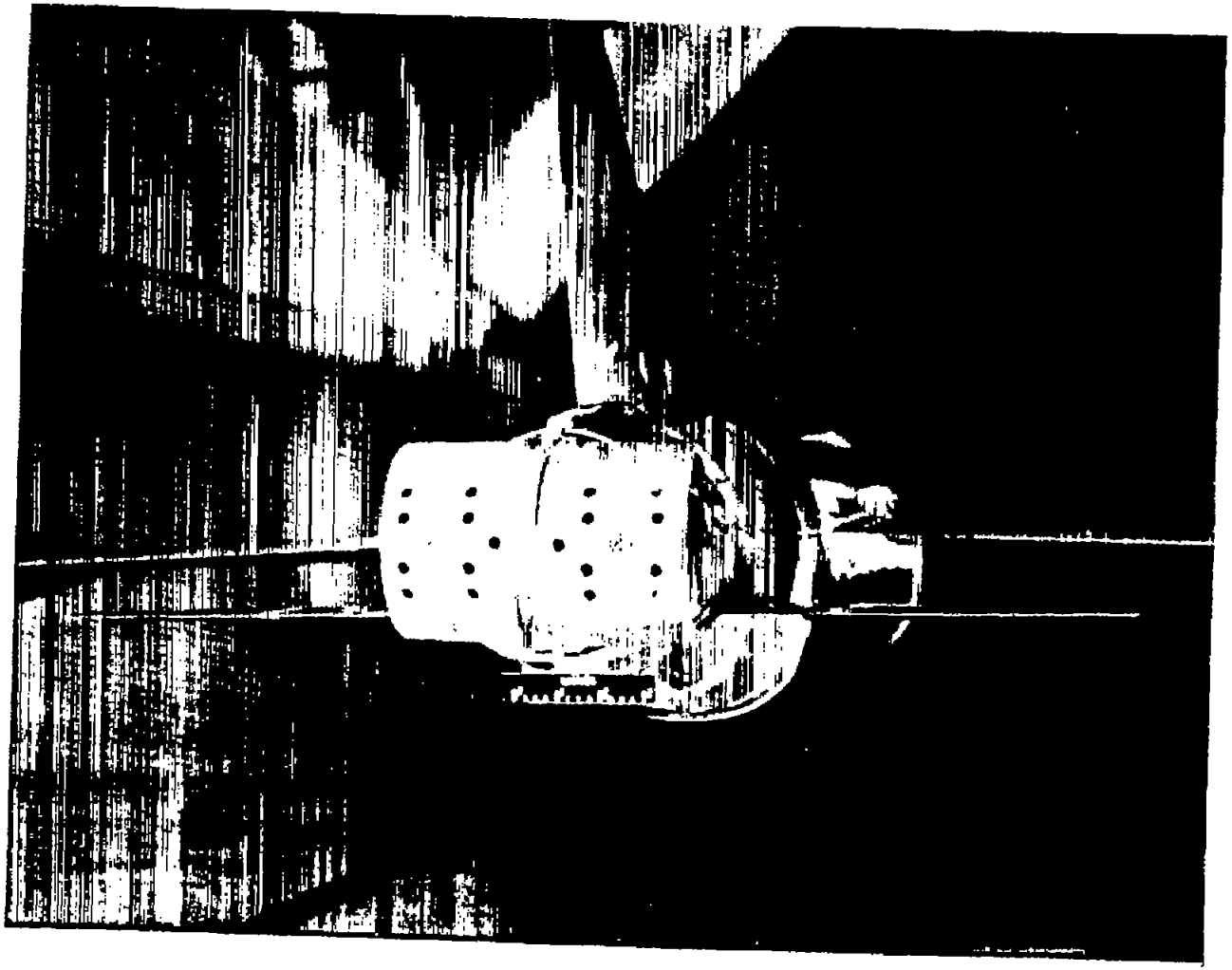

(f) Rear view, reverser perforated. L-95430

Figure 1.- Concluded.

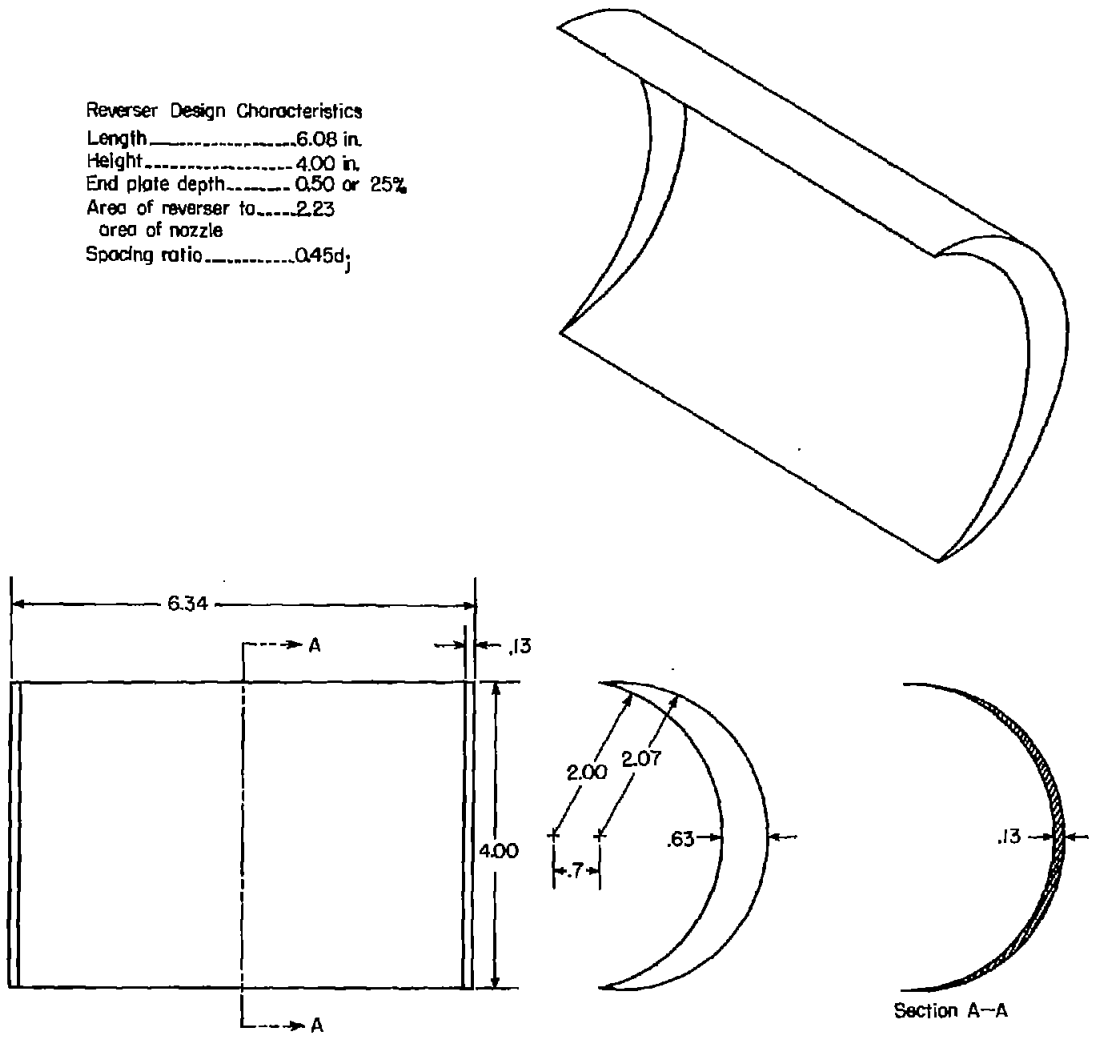

Figure 2.- Geometric details of target-type thrust reverser. All dimensions are in inches.

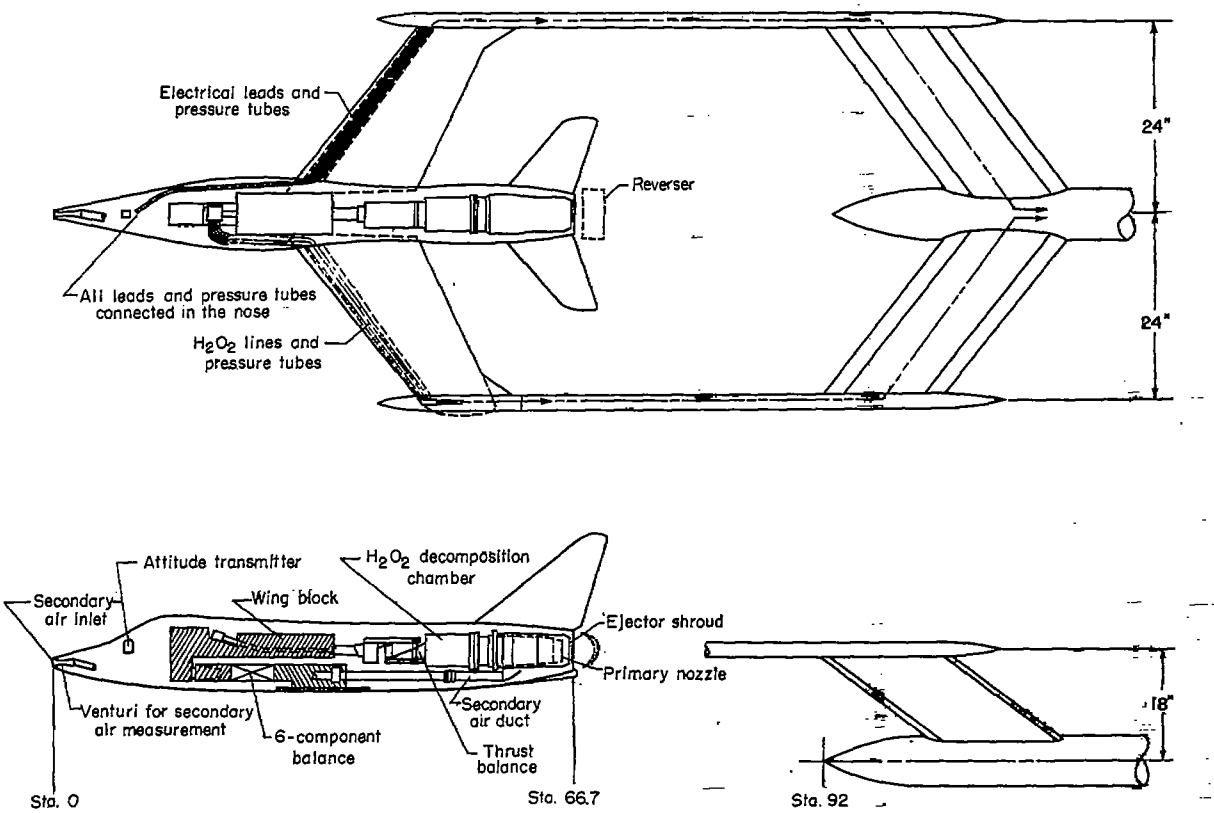

WING	
Wing area, (nominal), S	4.44 sq ft
AR	4.00
$\Lambda_{c/4}$	35°
c_r	17.273 in.
c_t	8.636 in.
NACA 65A006 airfoil sections-streamwise with 2.4 %c leading-edge camber	
Taper ratio	0.50
A_j/S (non-afterburning)	0.00839

FUSELAGE	
Length	66.7 in.
Max. height	9.0 in.
Max. width	8.6 in.
Area ruled for M = 1.0	

VERTICAL TAIL	
$\Lambda_{c/4}$	44°, 27°
Root section	NACA 0006
Tip section	NACA 0006
c_r	14.000 in.
c_t	2.480 in.
Taper ratio	0.18

HORIZONTAL TAIL	
$\Lambda_{c/4}$	35°
Root section	NACA 65A006
Tip section	NACA 65A004
c_r	9.893 in.
c_t	3.960 in.
AR	3.50
Taper ratio	0.40
i_t	-1.50°

(a) Complete model.

Figure 3.- Sketch of jet-exhaust simulator model and support system.

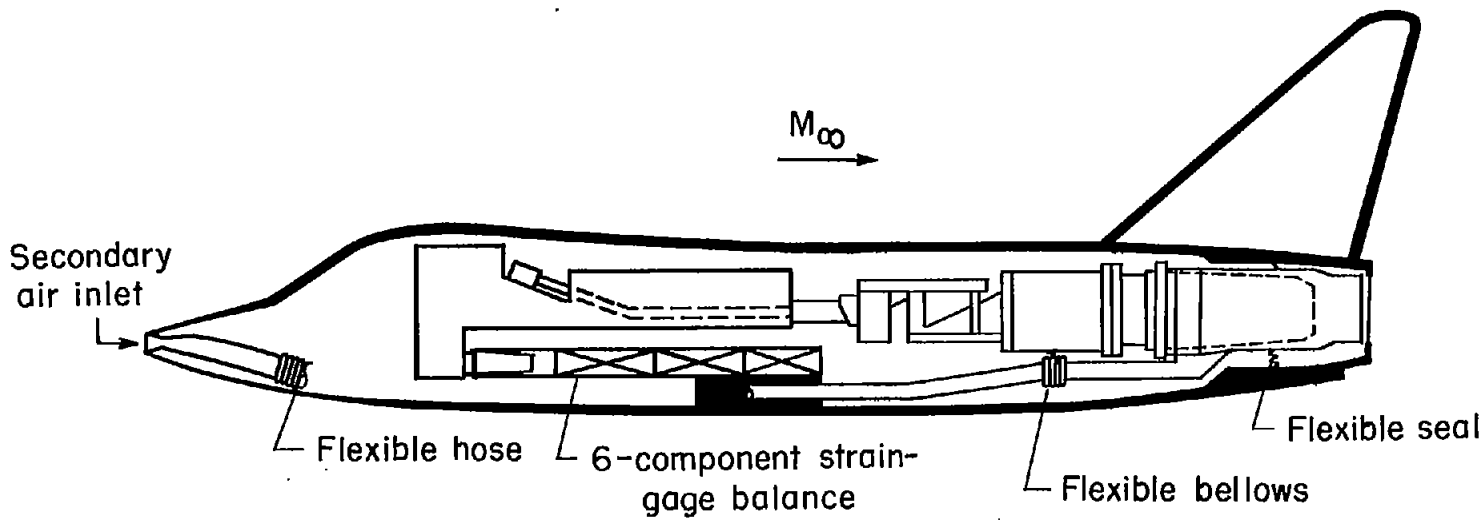

(b) External-drag system.

Figure 3.- Continued.

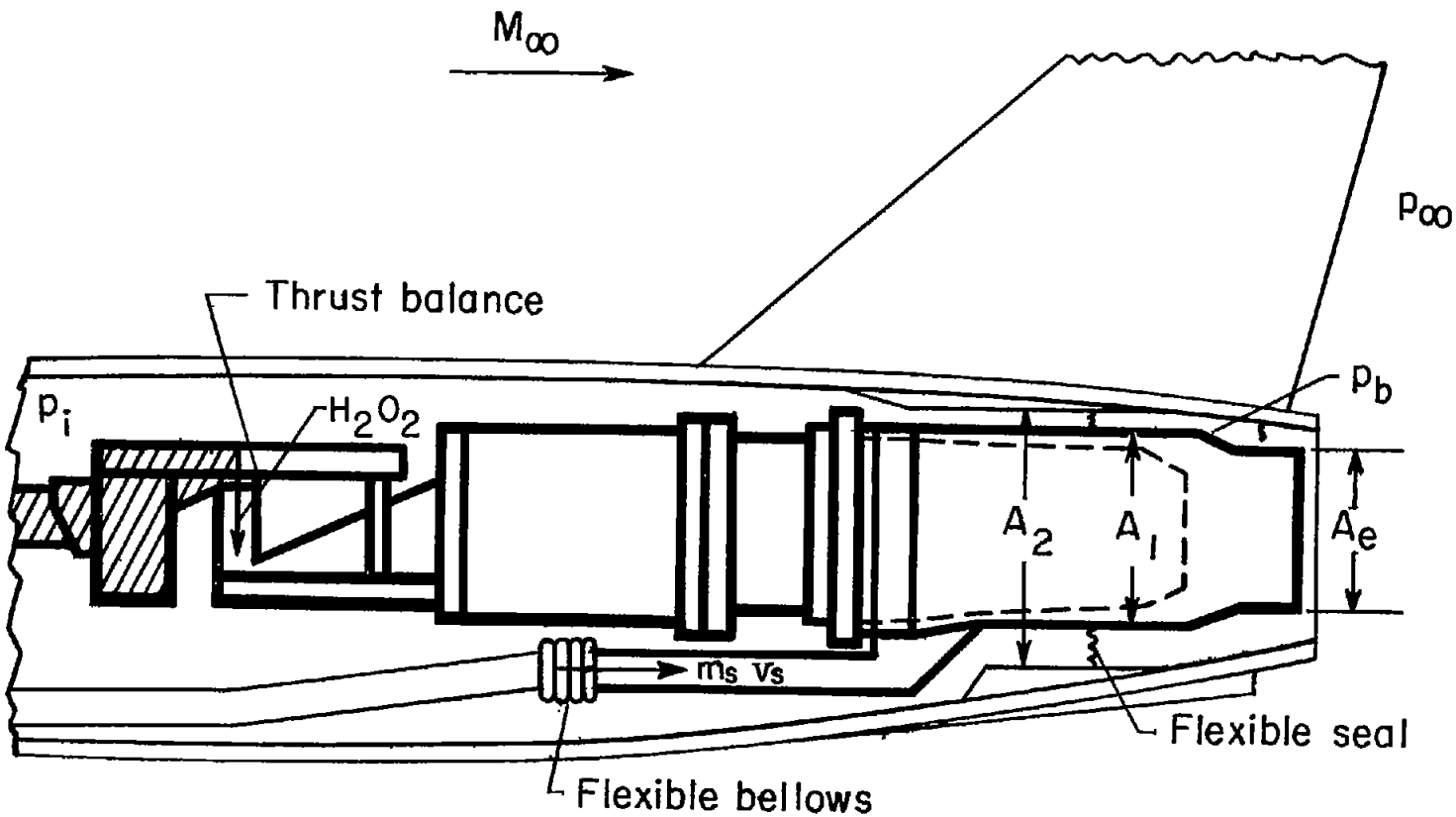

(c) Thrust system.

Figure 3.- Concluded.

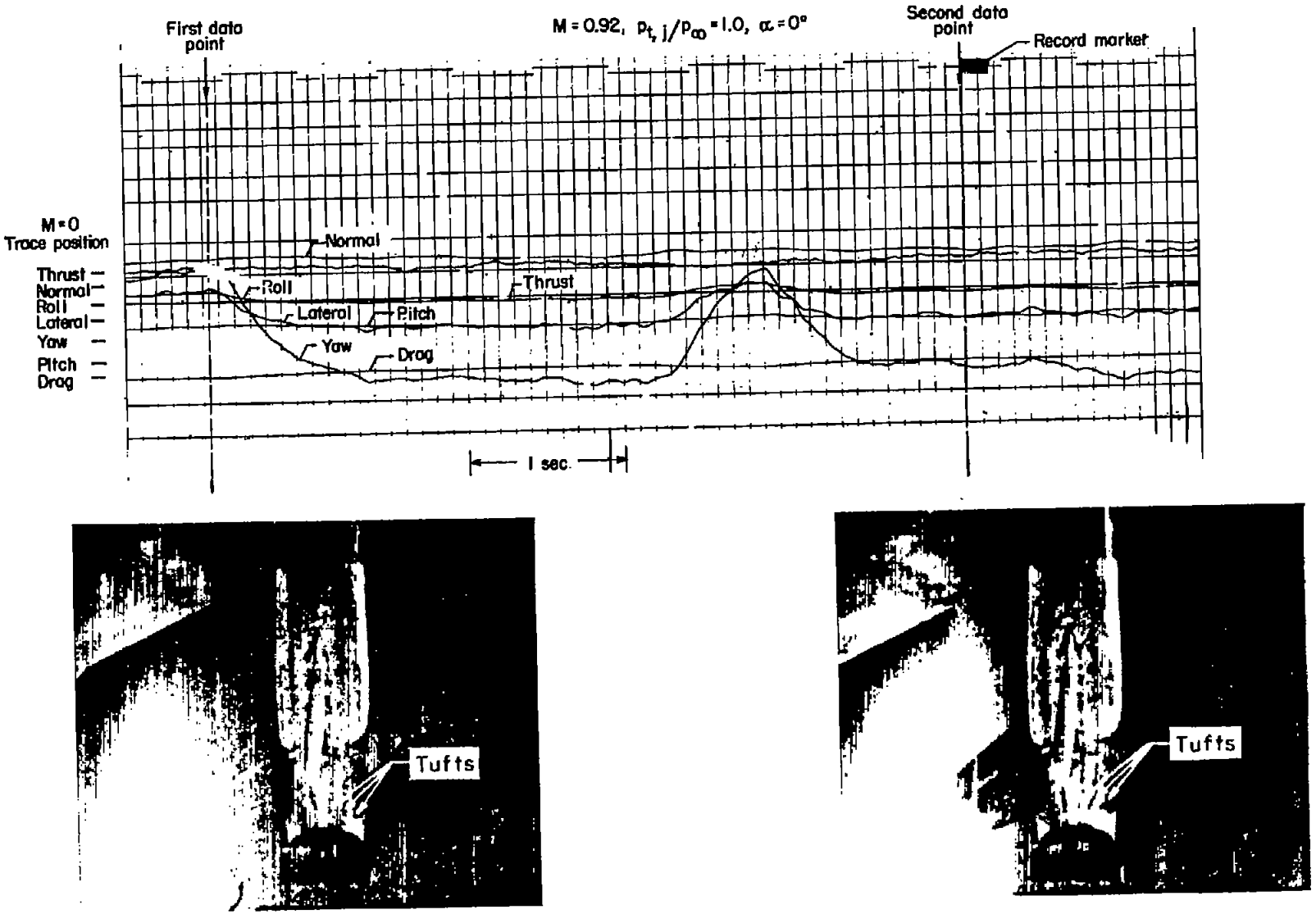

(a) Record and tuft pictures.

L-57-4442

Figure 4.- Oscillograph record of forces and moments with jet off; tuft pictures and pressures taken simultaneously.

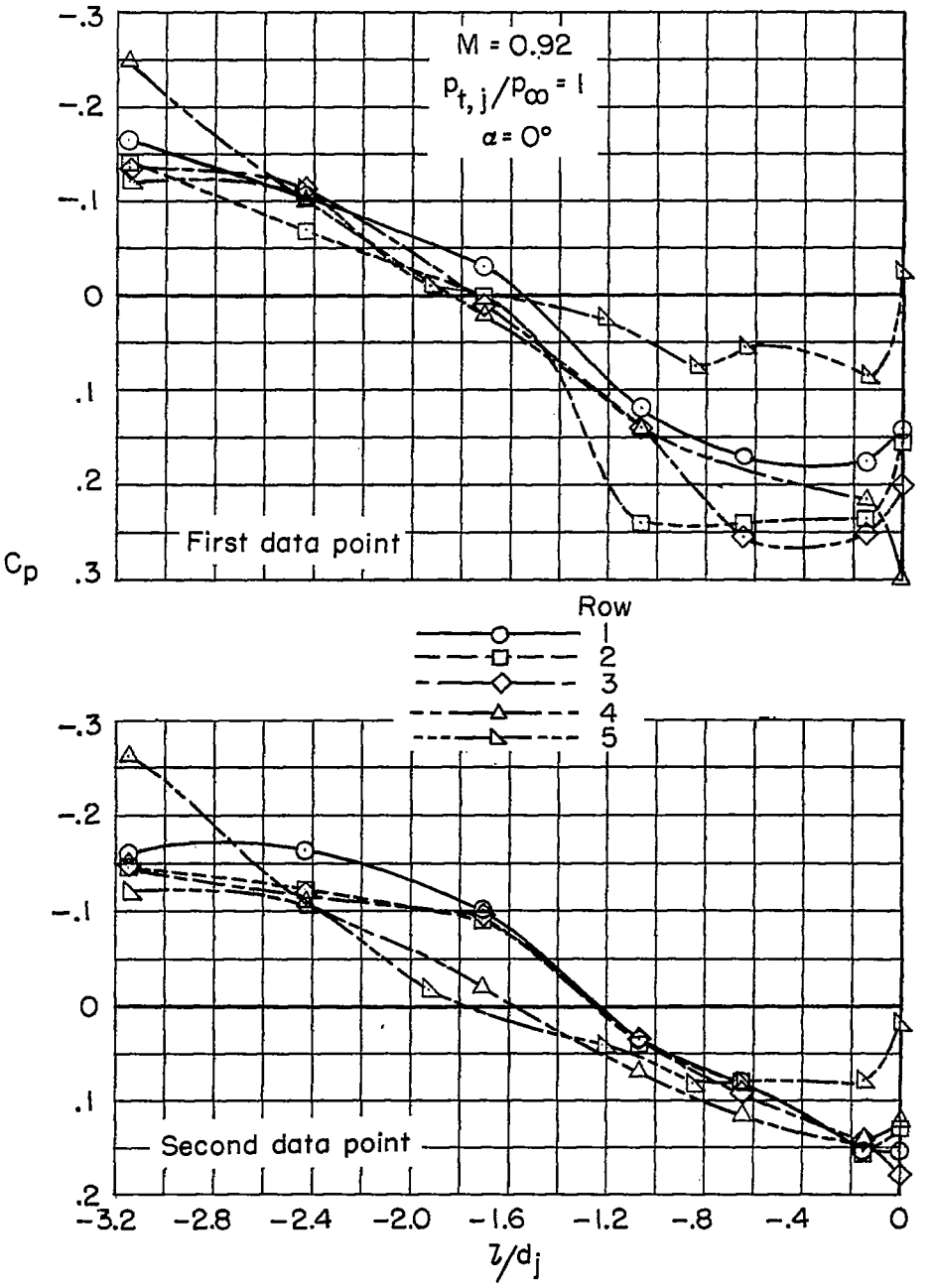

(b) Pressures taken at each point.

Figure 4.- Concluded.

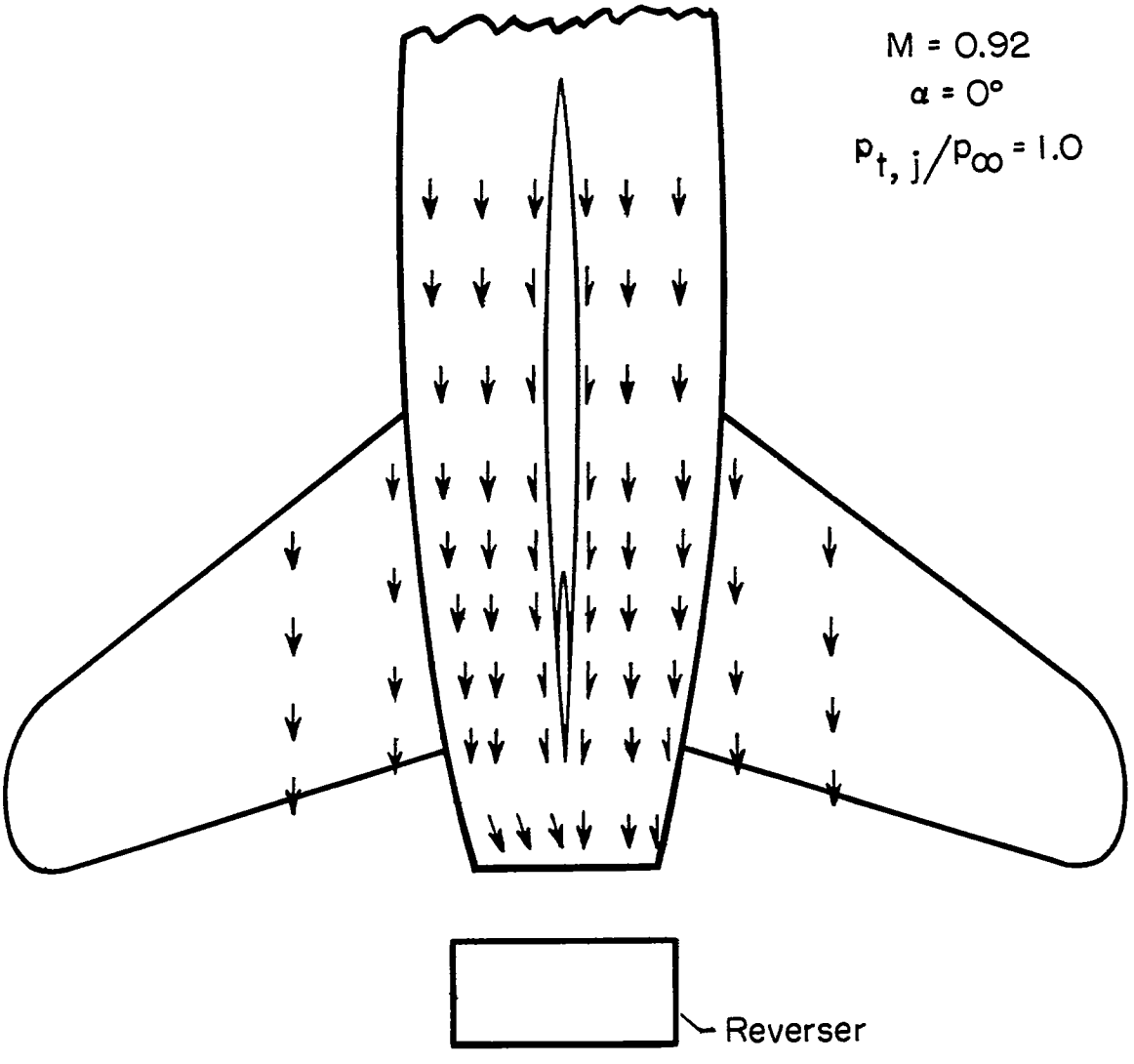

(a) Jet off.

Figure 5.- Tuft patterns on afterbody, reverser extended.

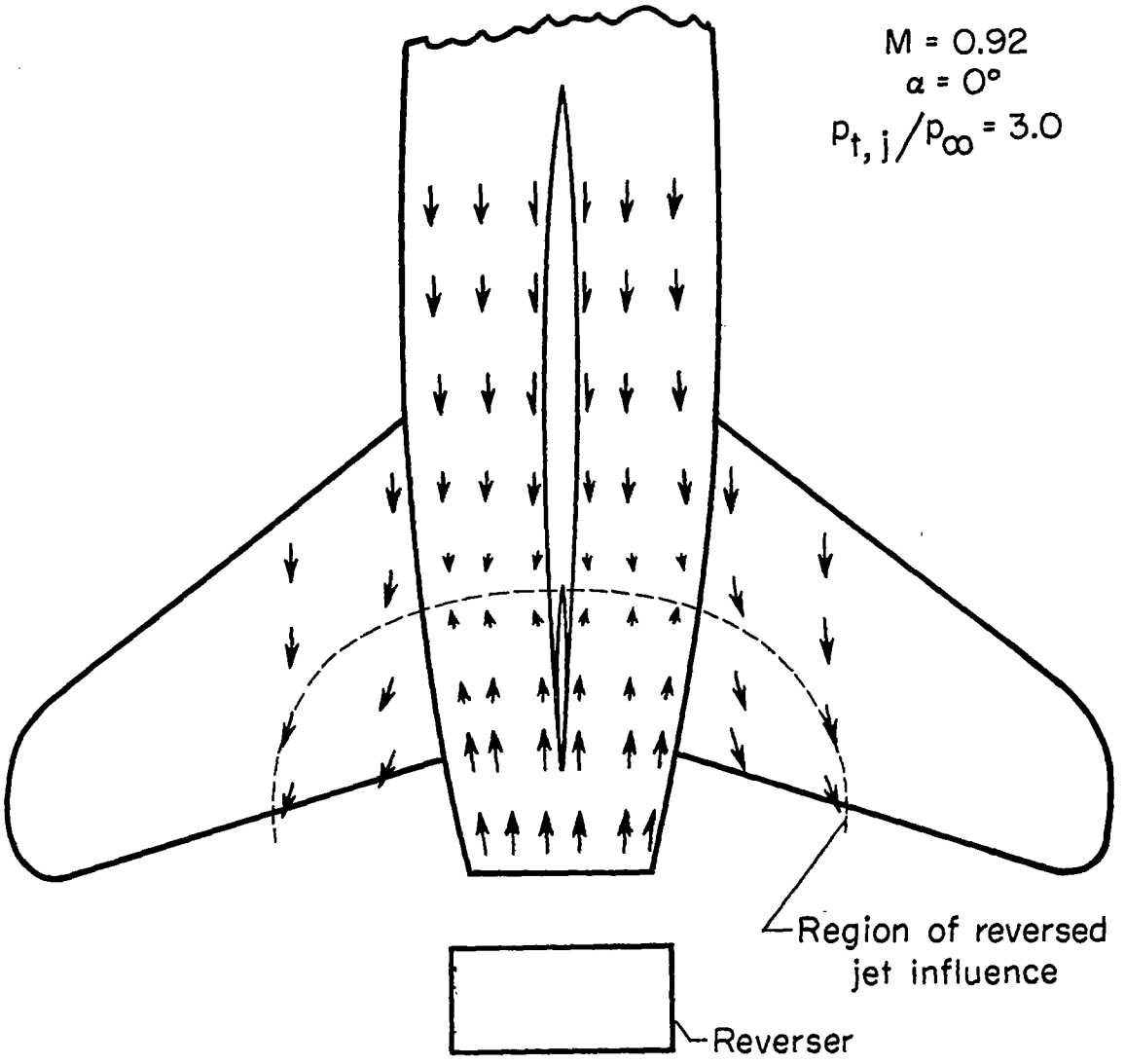

(b) Jet on.

Figure 5.- Concluded.

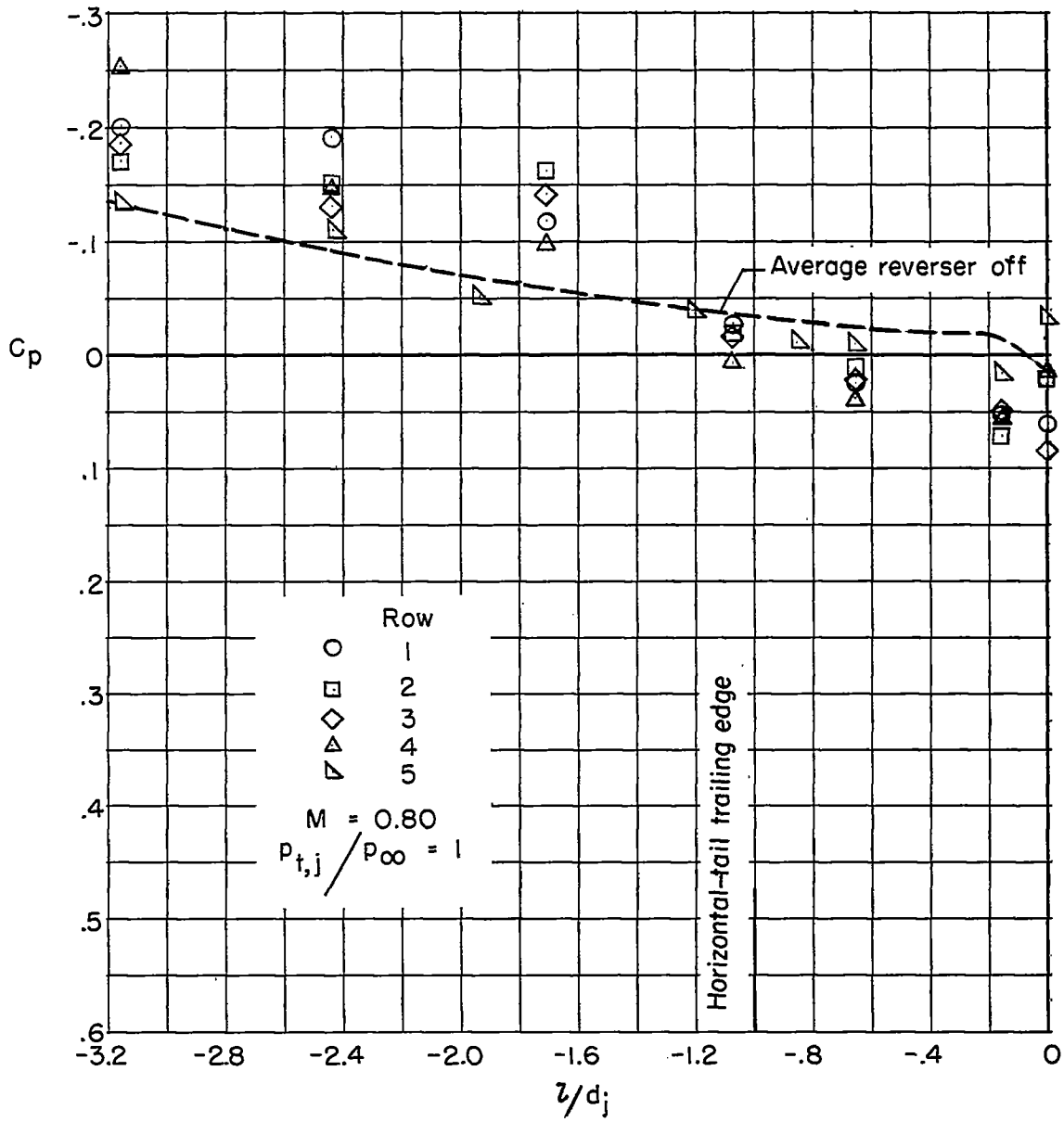

(a) M = 0.80.

Figure 6.- Variation of afterbody pressure coefficient with l/d_j for three Mach numbers and three jet total-pressure ratios at $\alpha = 0^\circ$. (Position of horizontal-tail trailing edge is indicated by solid line at $l/d_j = -1.0$.)

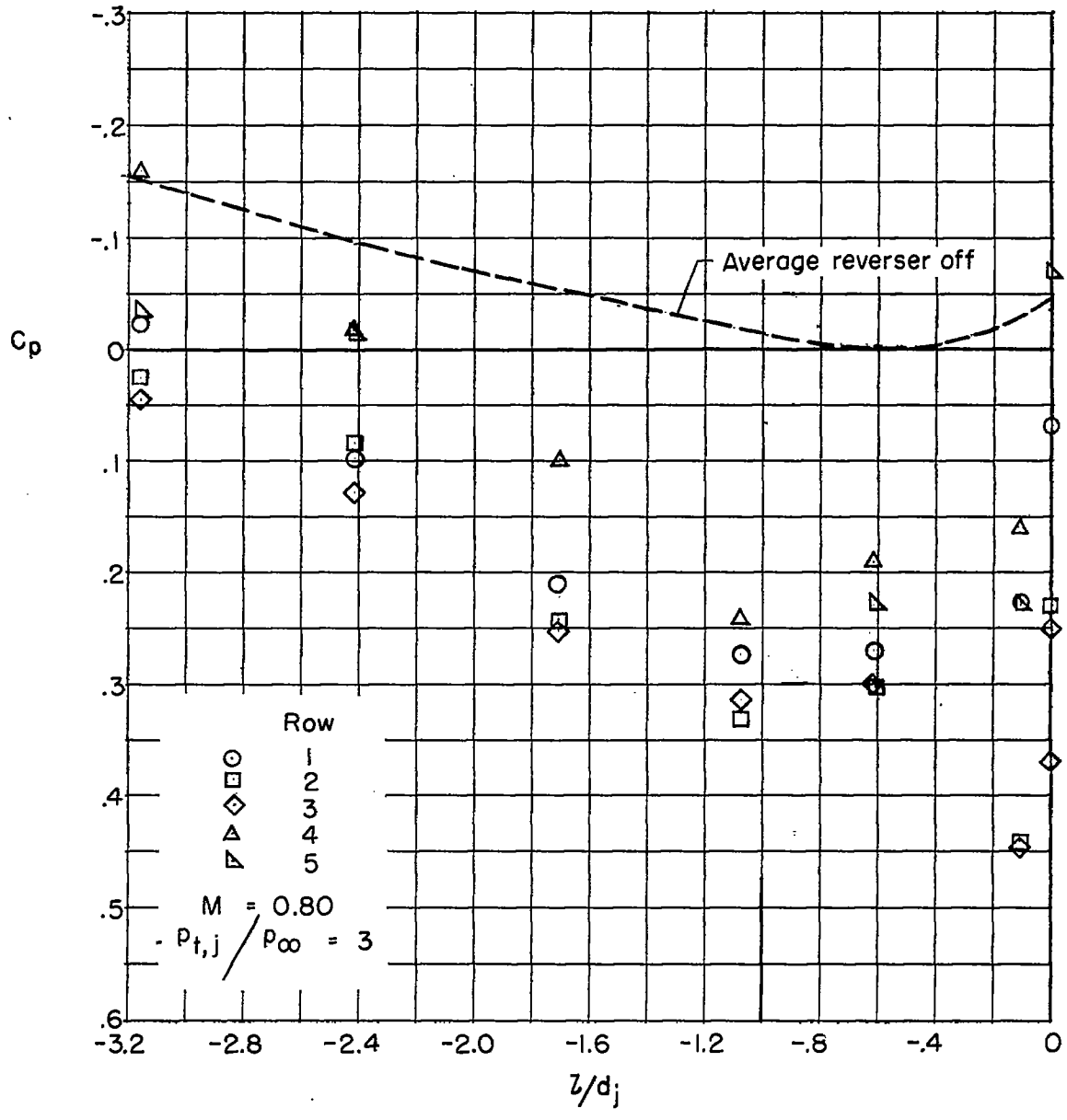

(a) M = 0.80, continued.

Figure 6.- Continued.

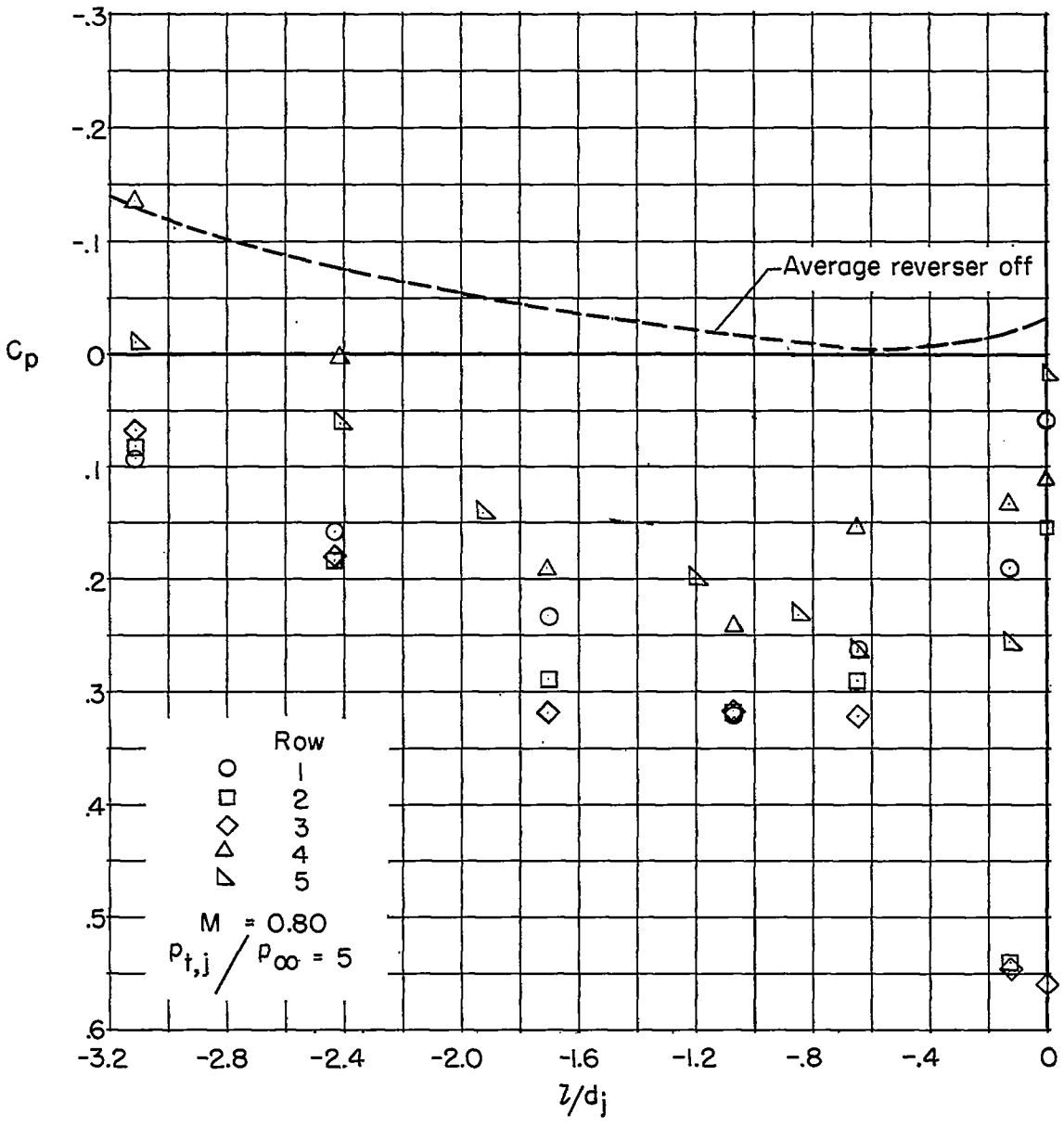

(a) M = 0.80, concluded.

Figure 6.- Continued.

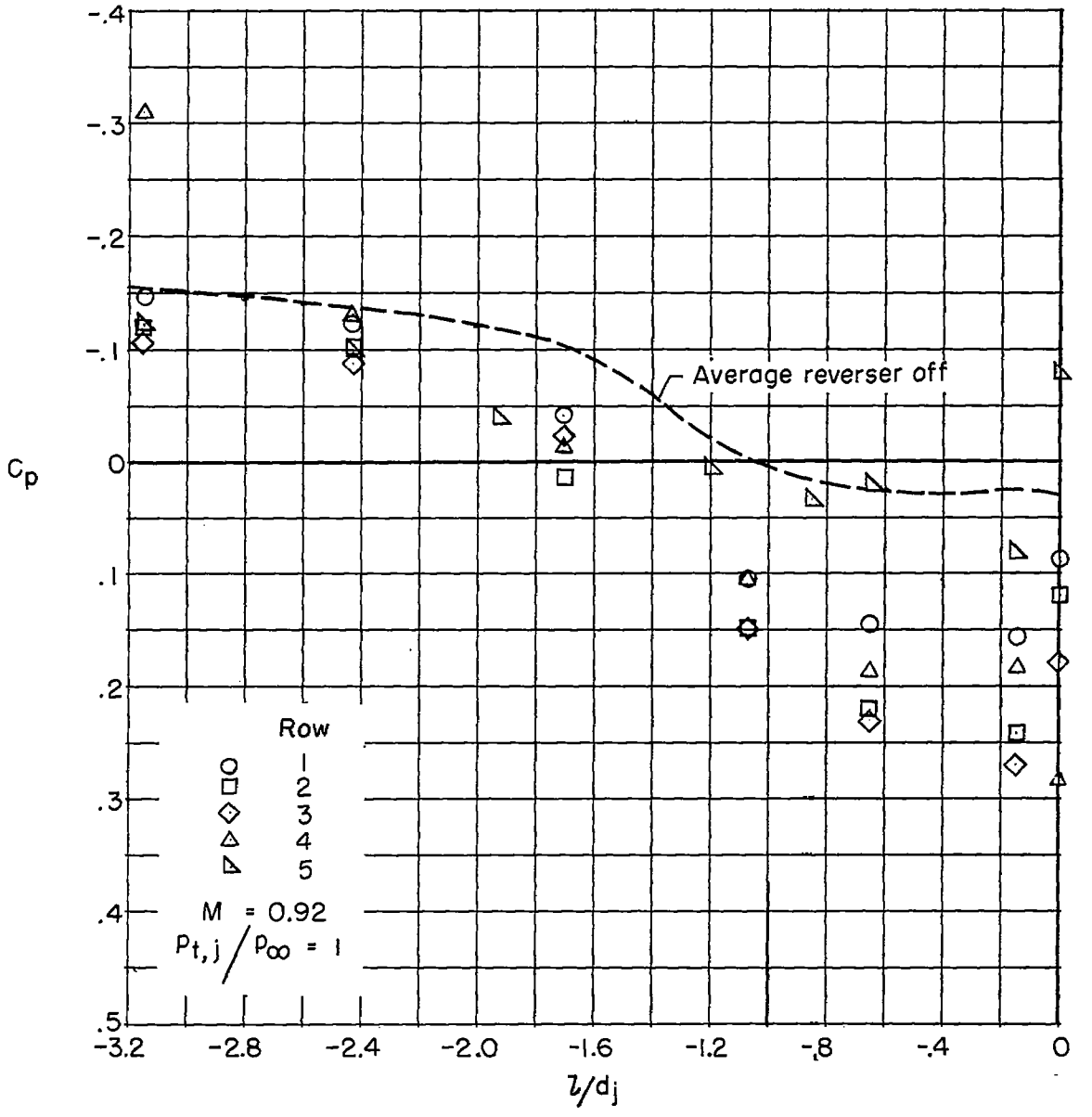

(b) M = 0.92.

Figure 6.- Continued.

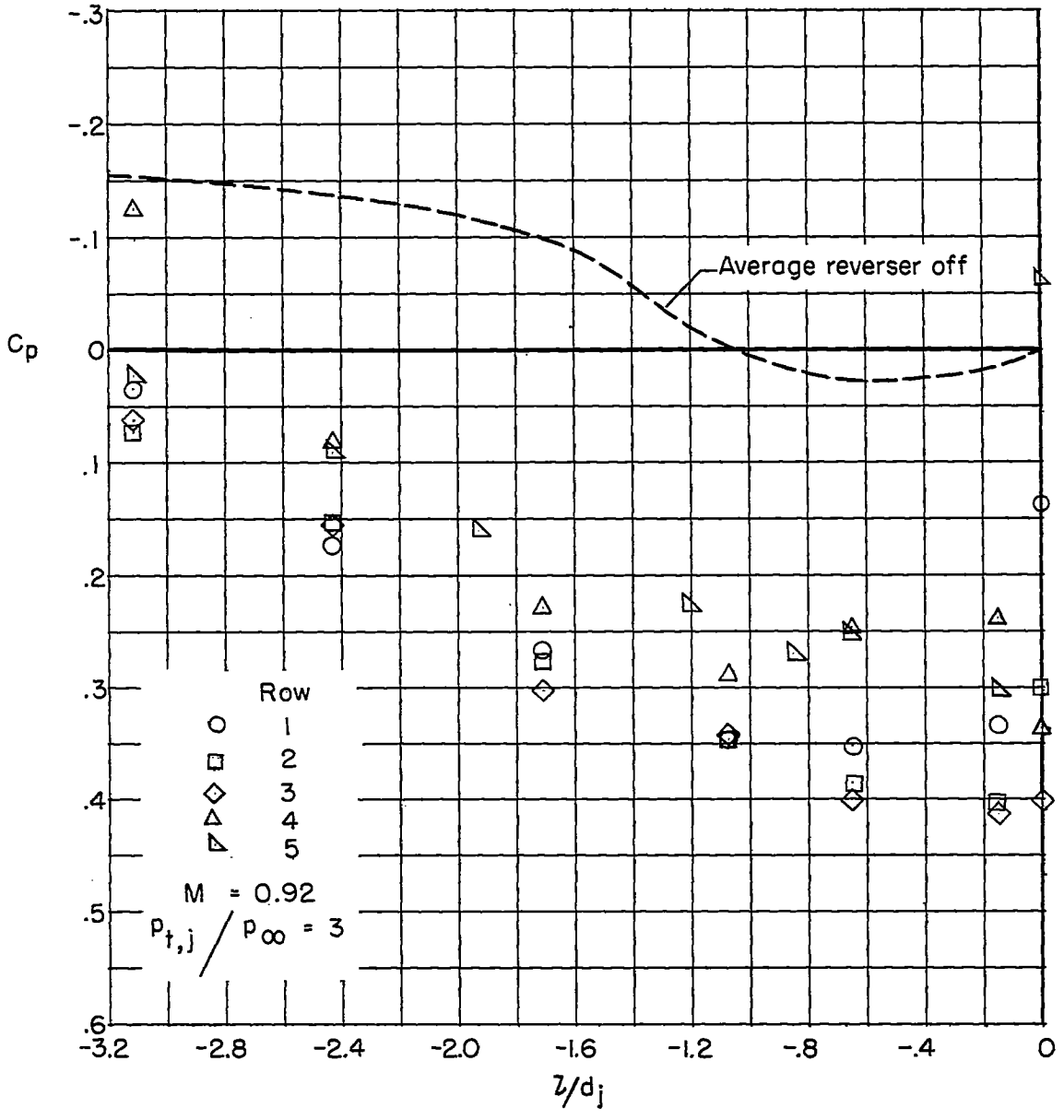

(b) M = 0.92, continued.

Figure 6.- Continued.

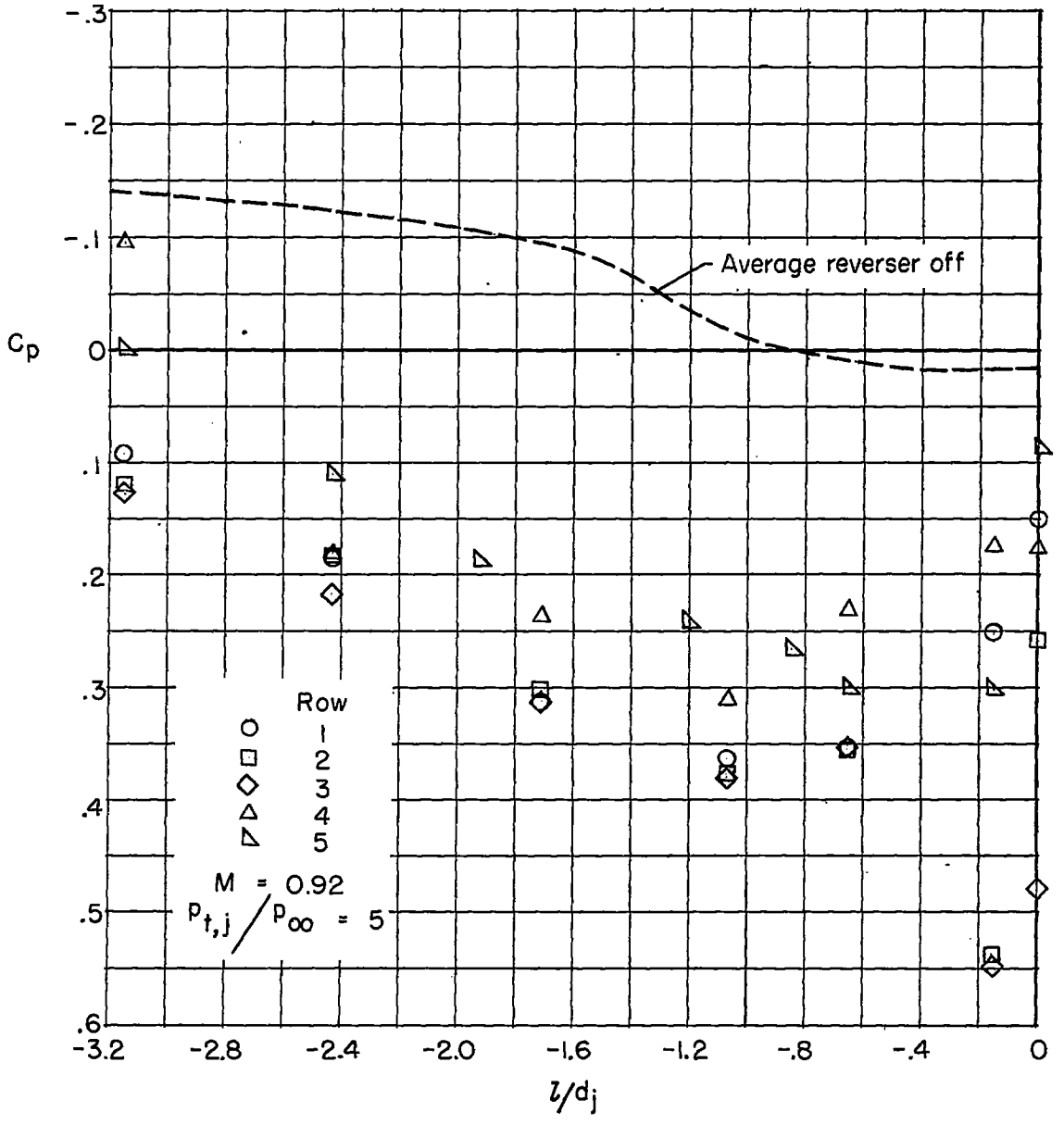

(b) M = 0.92, concluded.

Figure 6.- Continued.

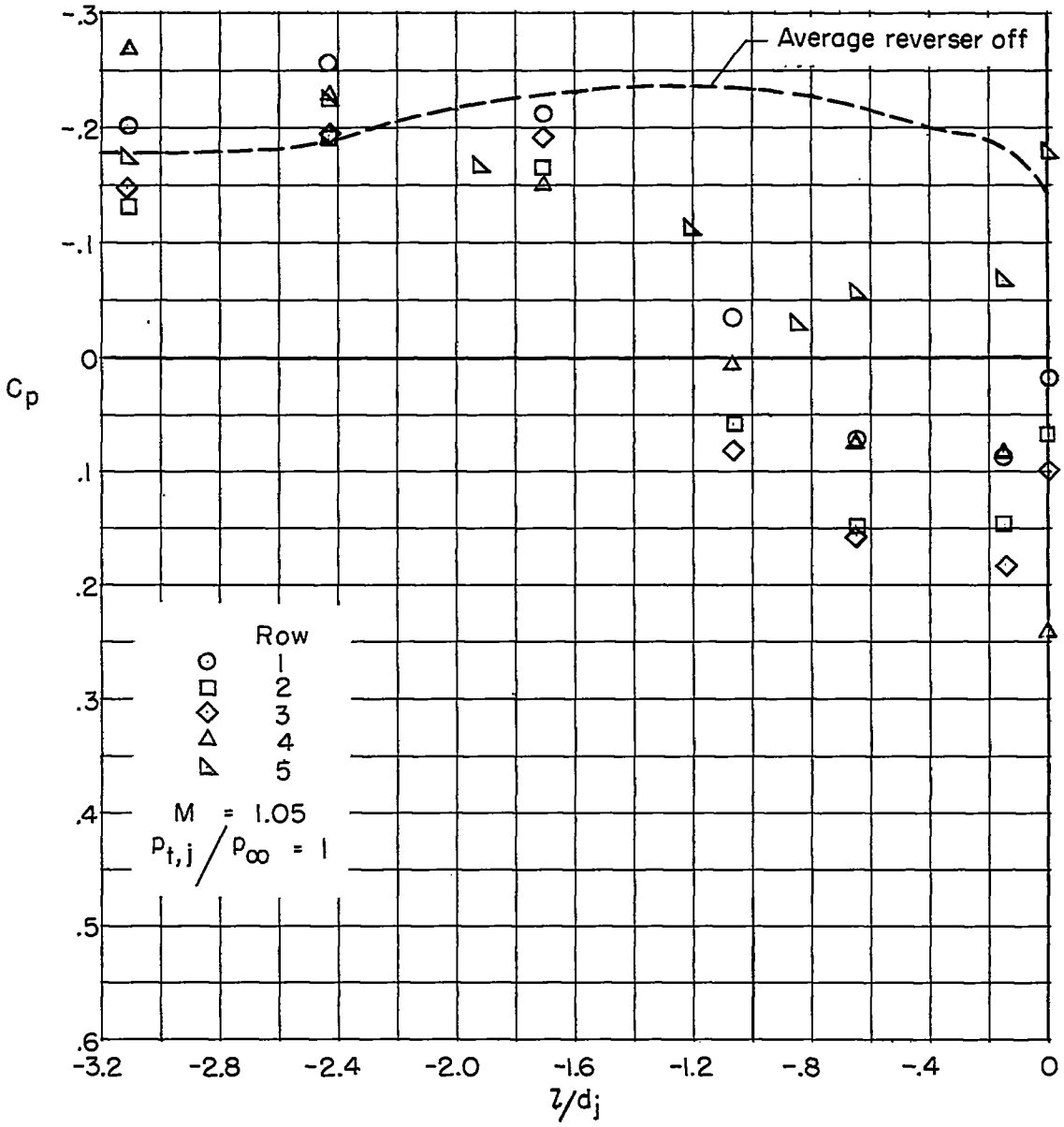

(c) M = 1.05.

Figure 6.- Continued.

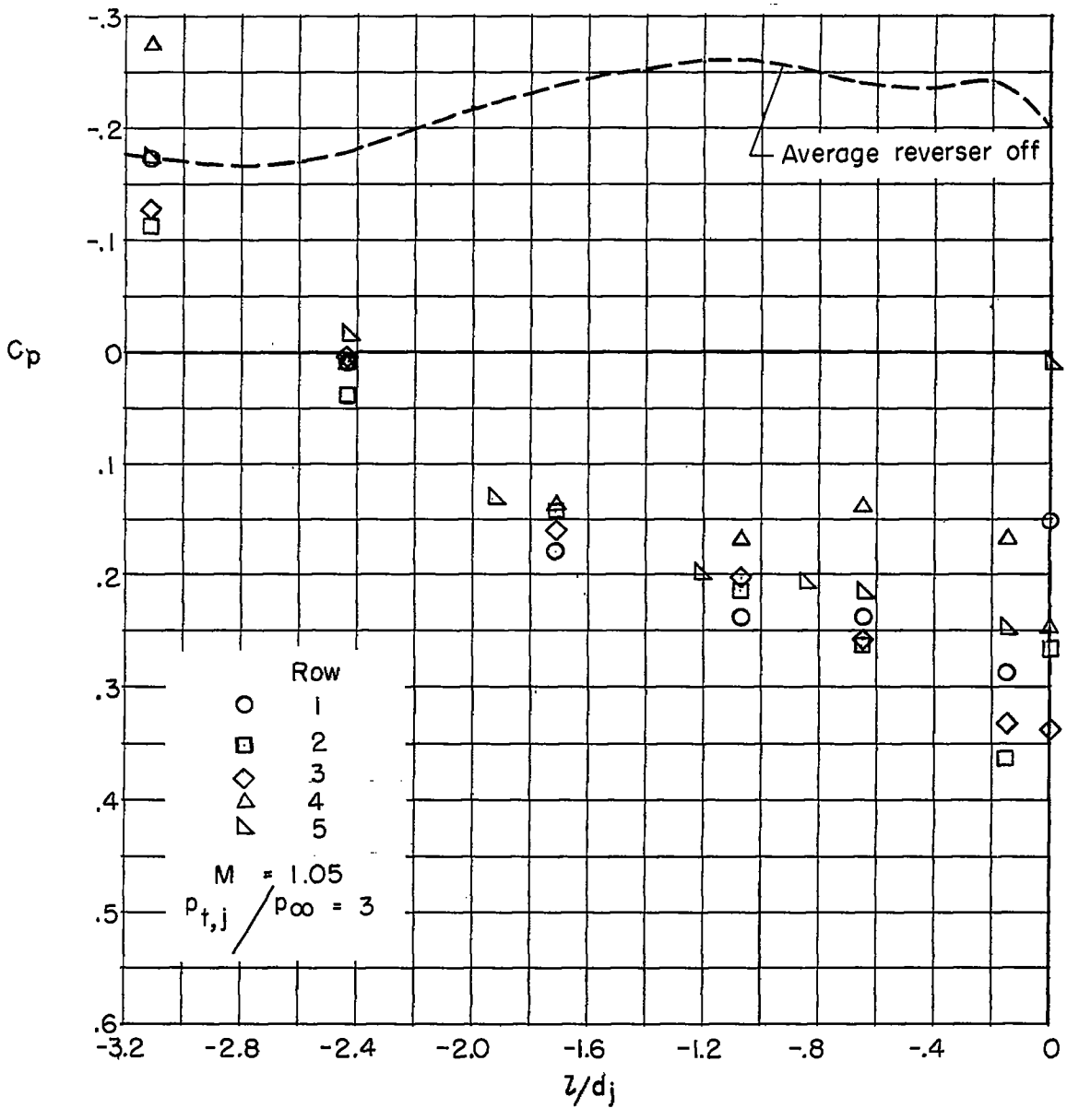

(c) M = 1.05, continued.

Figure 6.- Continued.

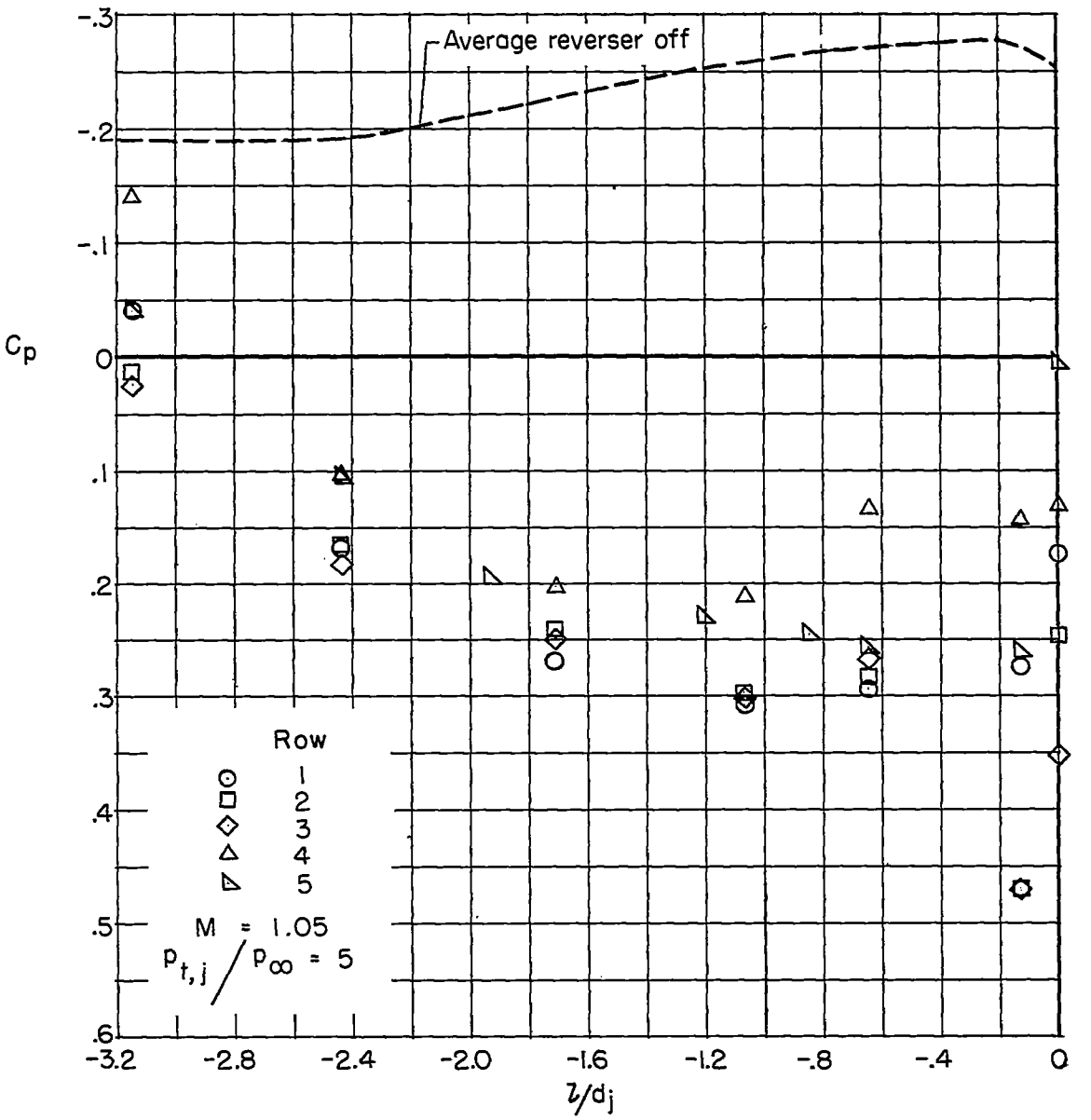

(c) M = 1.05, concluded.

Figure 6.- Concluded.

CONFIDENTIAL

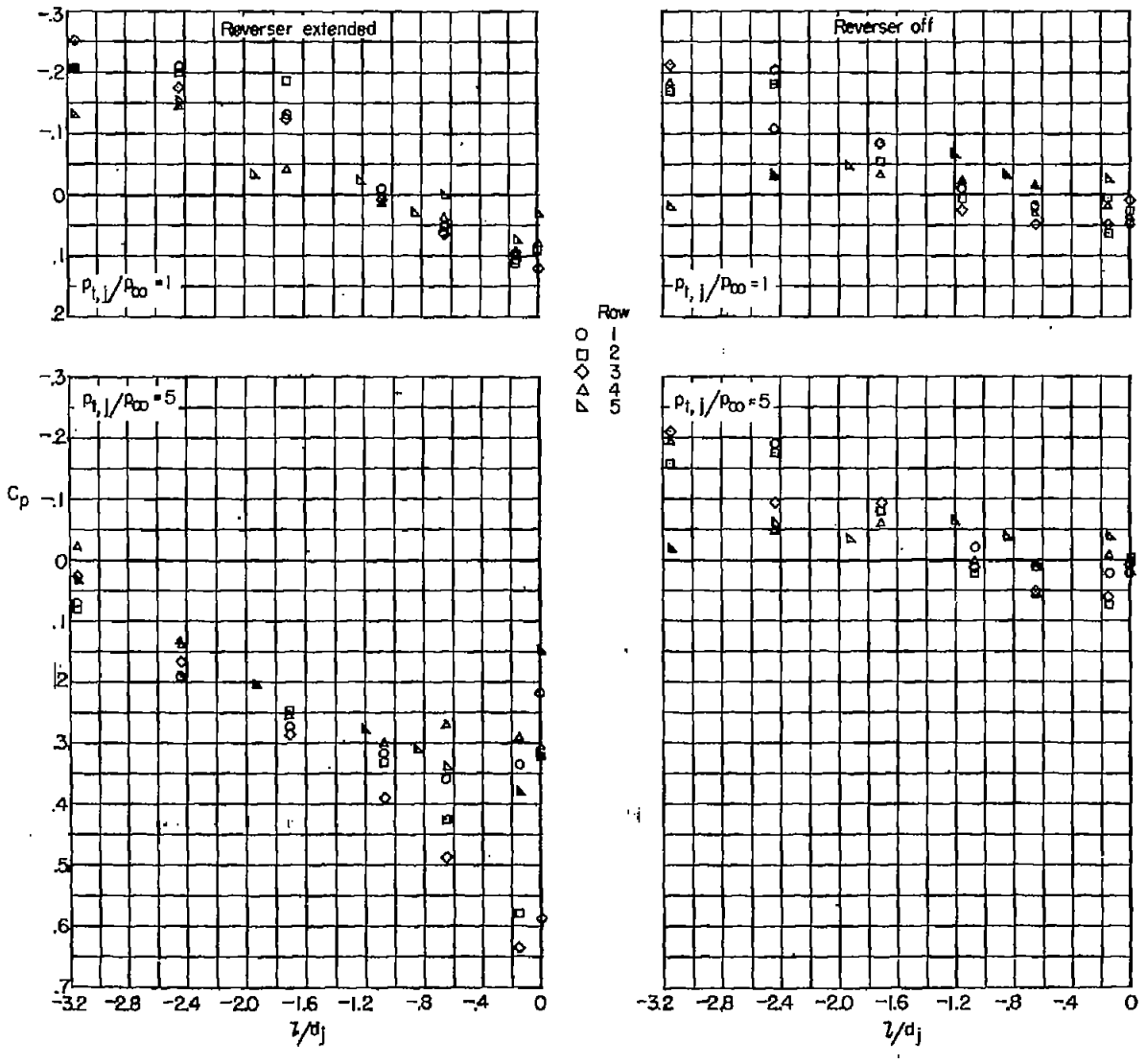

Figure 7.- Variation of pressure coefficient with afterbody length at $M = 0.92$ and $\alpha = 5^\circ$.

CONFIDENTIAL

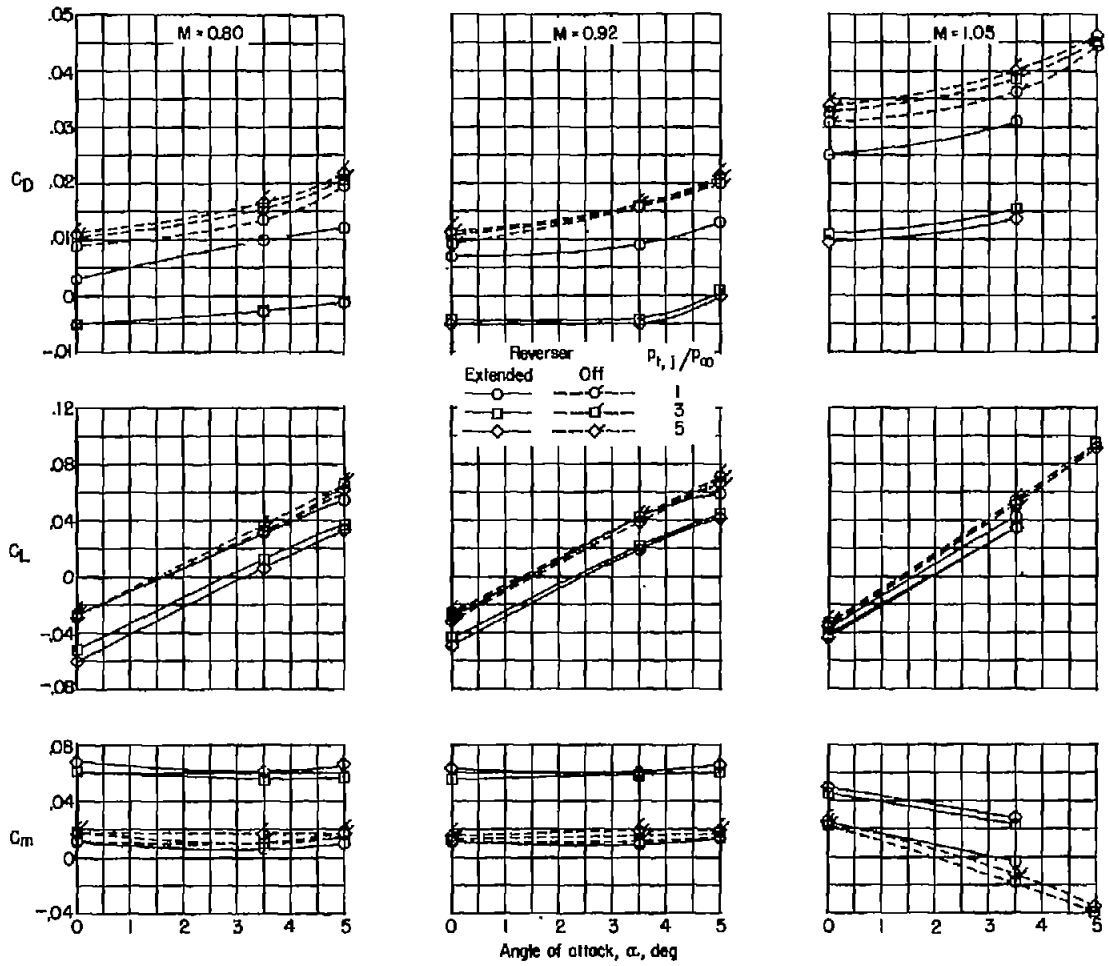

(a) C_D, C_L, and C_m plotted against α for constant values of $p_{t,j}/p_\infty$.

Figure 8.- Aerodynamic characteristics of fuselage-tail combination with and without a target-type thrust reverser.

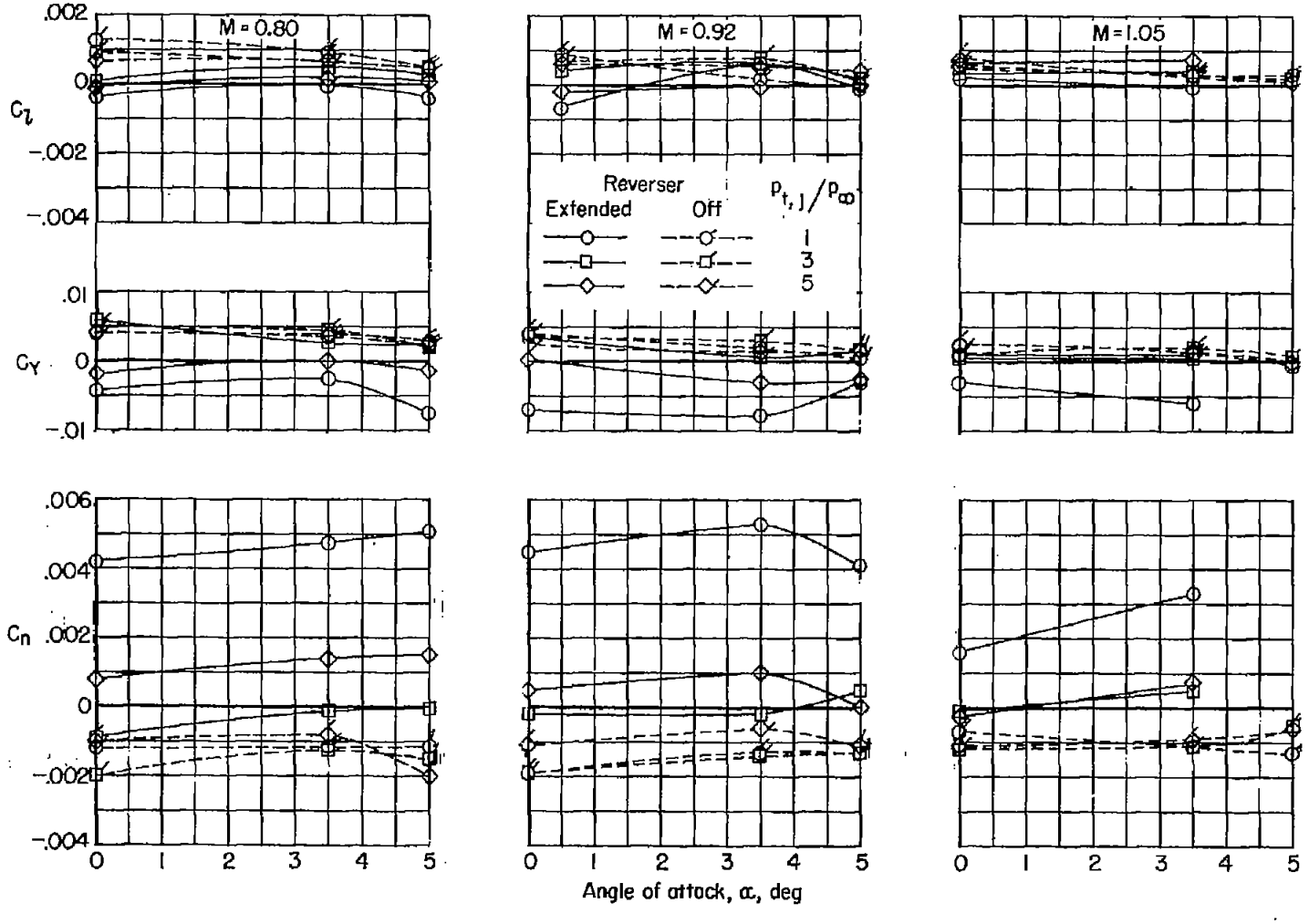

(b) C_l, C_Y, and C_n plotted against α for constant values of $p_{t,j}/p_\infty$.

Figure 8.- Concluded.

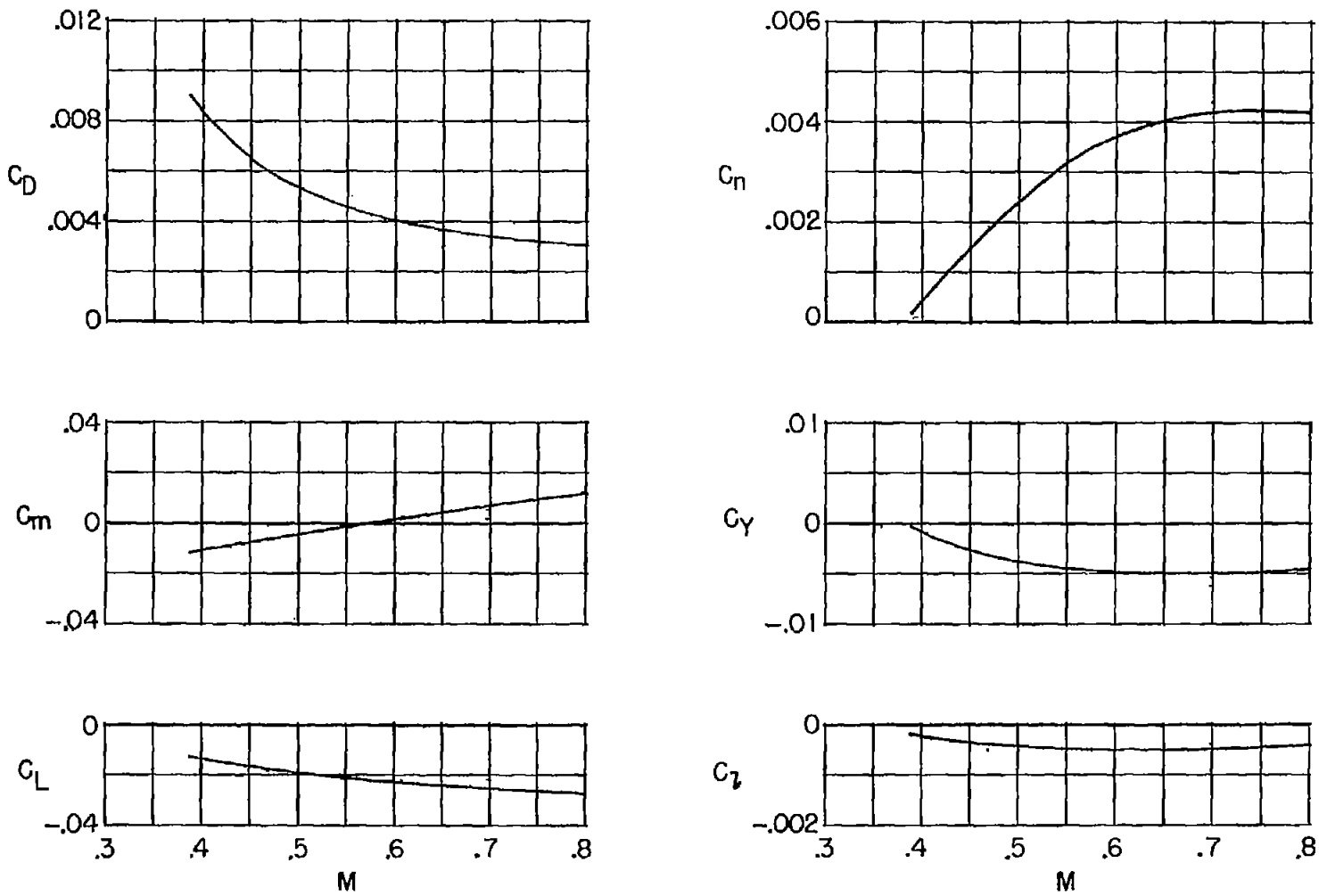

Figure 9.- Aerodynamic characteristics of fuselage-tail combination with reverser extended; $\alpha = 0^{\circ}$; jet off.

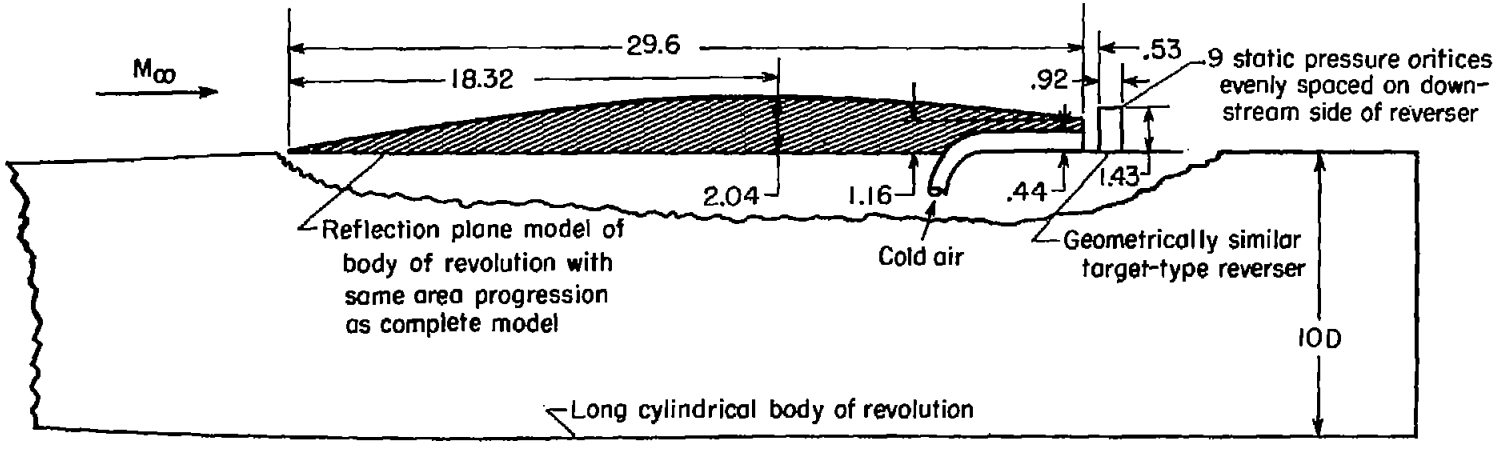

(a) Details of small-scale reverser model.

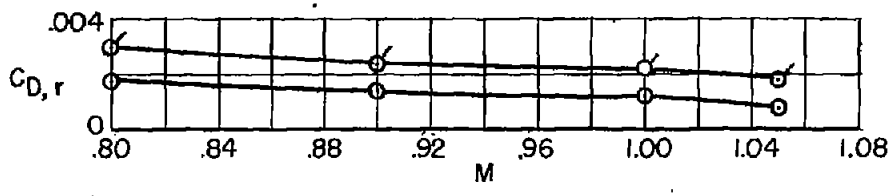

(b) Pressure drag on downstream side of small-scale thrust reverser. Flags indicate jet on at $p_{t,j}/p_\infty = 3.0$.

Figure 10.- Model details and pressure-drag coefficient on small-scale reverser model. All dimensions are in inches.